HEADWATER SEDIMENT DYNAMICS IN DEBRIS FLOW CATCHMENT: IMPLICATION OF DEBRIS SUPPLY USING HIGH RESOLUTION TOPOGRAPHIC SURVEYS

A. Loye[1], M. Jaboyedoff[1], J. I. Theule[2] and Frédéric Liébault[2]

[1]{Institute of Geomatics and Risk Analysis, University of Lausanne, Switzerland}

[2]{Université Grenoble Alpes, Irstea, UR ETNA, Saint-Martin-d'Hères, France}

Correspondence to: A. Loye (alexan2re.loye@gmail.com)

Abstract

Debris flows have been recognized to be linked to amounts of material temporarily stored in torrent channels. Hence, sediment supply and storage changes from low-order channels of the Manival catchment, a small tributary valley with an active torrent system located exclusively in sedimentary rocks of the Chartreuse Massif (French Alps), were surveyed periodically for 16 months using terrestrial laser scanning (TLS) to study the coupling between sediment dynamics and torrent responses in terms of debris flow events, which occurred twice during the monitoring period. Sediment transfer in the main torrent was monitored with cross-section surveys. Sediment budgets were generated seasonally using sequential TLS data differencing and morphological extrapolations. Debris production depends strongly on rockfall occurring during winter – early spring season, following a power law distribution for volumes of rockfall events above 0.1 m^3, while hillslope sediment reworking dominates debris recharge in spring and autumn, which shows effective hillslope-channel coupling. The occurrence of both debris flow events that occurred during the monitoring was linked to recharge from previous debris pulses coming from the hillside and from bedload transfer. Headwater debris sources display an ambiguous behaviour in sediment transfer: low geomorphic activity occurred in the production zone, despite rainstorms inducing debris flows in the torrent; still, a general reactivation of sediment transport in headwater channels was observed in autumn without new debris supply, suggesting that the stored debris was not exhausted. The seasonal cycle of sediment yield seems to depend not only on debris supply and runoff (flow capacity),

but also on geomorphic conditions that destabilize remnant debris stocks. This study shows that monitoring the changes within a torrent's in-channel storage and its debris supply can improve knowledge on recharge thresholds leading to debris flow.

1 Introduction

In steep mountain catchments, rainfall intensity and duration (incl. snowmelt) are insufficient to predict debris flow occurrence, even though initiation of runoff-generated debris flows requires significant water inflow (Van Dine, 1985; Decaulne and Saemundsson, 2007; Guzzetti, 2008). In many cases, the properties of the channel reach which determine the amount of debris that can be entrained can be often more important than the mechanisms of initiation induced by the hydrological/meteorological conditions prior to event (Hungr, 2011; Theule et al., 2015). The frequency and magnitude of debris flow have been recognized to be linked to the amount of material temporarily stored in channel reaches (Van Steijn et al., 1996; Cannon et al, 2003; Hungr et al. 2005), such that hillside sediment delivery, recharging those channels, represents a key factor for the occurrence of debris flows (e.g. Benda and Dunne, 1997; Bovis and Jakob, 1999; Berti et al., 2000). This implies efficient hillslope – channel coupling (Hooke, 2003; Schlunegger et al., 2009; Johnson and Warburton, 2010). Therefore, the rate of sediment supply needs to be considered for predicting debris flow hazards (Rickenmann, 1999; Jakob et al., 2005). However, the difficulty results in quantifying sediment processes and rates and volumes from hillslopes and in-channel debris storage (Peiry, 1990; Zimmermann et al., 1997).

Quantification of overall sediment production and transfer rate has increasingly relied upon multi-temporal digital stereophotogrammetry (Coe et al., 1993; Chandler and Brunsden, 1995; Veyrat-Chavillon and Memier, 2006) and elevation difference from High Resolution Digital Elevation Models (HRDEM) (Smith et al., 2000; Wu and Cheng, 2005; Roering et al., 2009; Theule et al., 2012). In terrain dominated by steep slopes, traditional aerial derived DEMs typically remain inappropriate to study geomorphic processes. Limitations include the poor rendering of small topographic changes (Perroy et al., 2010), poor representation of steep terrain with small curvature radii and data gaps in vertically oriented and overhanging topography. Even on gentler gradients, the sharp breaks in slope, encountered in erosion scars for instance, are often insufficiently modelled by airborne HRDEM, leading to erroneous volume estimations (Bremer and Sass, 2011). This represents a serious drawback in

estimating the sediment budget of steep terrain, where sediment activity comes mostly from rock walls and rugged gullies. Because of these issues, many hill- and rock-slope process studies have used terrestrial laser scanner (TLS) data to build the topographic model (Jaboyedoff et al., 2012). The recent development of long range TLS devices provides an effective means of acquiring high resolution topographic information that can adequately reflect the morphology of steep bedrock-dominated areas. The practical disadvantages in data acquisition inevitably related to ground surveys can be compensated for by flexibility in transport, ensuring a full coverage with minimal zones of topographic shadowing.

This paper presents a quantitative study of sediment recharge and channel response leading to debris flow events, using 3-D digital terrain models acquired by TLS. This is illustrated on the Manival (French Alps), a torrent that experiences runoff-generated debris flow almost every year (Péteuil et al., 2008). The surveys captured hillslope processes and sediment dynamics occurring throughout the system including the tributary channels down to the main torrent and were performed periodically over 16 months. The spatio-temporal variability of debris production and subsequent transport and storage of sediment are analysed on a seasonal time scale, in order to discuss the debris supply dynamics and the implications in debris flow initiation. This study also complements a parallel investigation regarding the controls on debris flow erosion and bedload transport in the Manival's torrent (Theule et al. 2015).

2 Study site

2.1 General setting

The 3.9 km^2 Manival catchment located at the edge of the Chartreuse massif (France) (Fig. 1) has a rugged, 1200 m relief watershed, resulting from deep headward entrenchment (Gidon, 1991). The topography consists of a narrowly-confined head and a steep-sided colluvium-filled valley, delimited in the west by a series of rock walls and scree-mantled deposits separated by rock couloirs, and in the east by steep rock and talus slopes divided by gullies. The lithology ranges in age from late Jurassic to early Cretaceous (Fig. 2) (Charollais et al., 1986). In the heart of the basin, thick sequences of calcareous marl interbedded with layers of marl predominate. Towards the ridge, the bedrock evolves progressively from stratified to more massive limestone. The valley sides are formed by the fold limbs of an anticline, where secondary folding and minor faults induce local variations in structure (Gidon, 1991). This

tectonic setting and the varying stratigraphic competency have strongly influenced the topographic development of the catchment, providing a dynamic geomorphic environment producing considerable runoff as a response to heavy frequent rainstorms (Fig. 3).

2.2 Characteristics of the headwater sediment dynamics

The contemporary geomorphic activity contributing to the torrent's recharge with debris is concentrated exclusively in the headwater, where no remnant glacial deposits are found (Gruffaz, 1997). In the upper catchment, large old rock deposits flooring the west side hillslope (Fig. 4) have dramatically influenced the bottom topography, and thus the channel network, resulting in a conjunction of four first-order debris flow channels deeply incised down to the bedrock in several reaches. The upper catchment can therefore be subdivided in five subcatchments in terms of sediment recharge (Fig. 2). Bed entrenchment is now constrained by check dams. However, lateral erosion still occurs episodically by flooding and debris flow scouring.

The style of sediment production and delivery is somewhat different throughout the headwater, according to the local morphology and the lithologic and structural setting. The major geomorphic processes, identified preliminarily by observations from aerial photographs and field investigations, were initially characterized in a map (Fig. 4) describing the spatial distribution of geomorphic features and sediment transfer processes contributing to debris recharge in the first-order channels. The west and upper sides are dominated by rockfall. Large rock collapses delimited by persistent joints occur due to the progressive degradation of the slope underneath (Loye et al., 2011). Where the slope gradient allows scree and soil development, erosion scars can be observed; sediment sources are remobilized from discrete shallow landslides. Depending on the location and size, rockfall can reach the channels directly, or accumulate on slopes or in ravines, before being subsequently routed to high-order segments by a combination of gravitational and hydrological processes. Towards the east, the erosion seems to be more progressive through the formation of gullies (Loye et al., 2012). Near the ridge, the slopes display mostly talus and scree deposits lightly covered with vegetation, whereas the hillside below exposes steepened rock slopes. Many active erosion scars can be observed. They contribute debris into gullies and talus slope deposits that are subsequently entrained in channels downslope.

Historical records of debris flows since the 18th century show a frequency of 0.3 events per year that reached the apex of the fan (Brochot et al, 2000). The largest event deposited approximately 60,000 m^3. However, the torrent experiences smaller fluxes of debris (<1,000 m^3) usually not reported in archives. Such events can occur 2-3 times per year, when initiated by intense runoff (Veyrat-Charvillon, 2005). Volumes of debris deposited in the sediment trap for the last 25 years are on average 2,200 m^3/yr, reaching a maximum of 7,000 m^3/yr in 2008 (RMT service).

3 Methods and data processing

3.1 Topographic monitoring using TLS

The terrain was surveyed with an ILRIS-3D laser scanner (Optech Inc.). This device provides a range up to 1.2 km for 80% reflectivity surface and the instrumental precision is about 7 mm/100 m range for both distance and position (Optech Inc.). The overall coverage of the upper catchment with TLS point clouds required 50 scans using a 20% surface overlap. These scans were collected over a 5-day period from 9 individual viewpoints to ensure a full 3-D rendering of the topography. Particular attention was given to irregular regions and major breaks in slope, such as rock couloirs and deep-cut gullies. Using multiple scanning locations allowed us to limit shadow zones and increase the point cloud density of the scanned area. A series of 4 surveys was performed for each season during 2009 and one extra survey was performed in July 2010 to analyse the effect of the preceding winter period (Table 1). The monitoring setup remained similar for all surveys. Post-processing of the TLS raw data was done using Polyworks (InnovMetric). Erroneous points and vegetation were filtered manually, ensuring a total control of the removed data to preserve a high density of points in topographic features with small radii curvature. Although this procedure is time consuming, (semi-)automatic approaches to filter vegetation accurately still remain in a stage of development for dissected mountain morphology (Brodu and Lague, 2012). Each of the multiple scans of a survey were merged to one another using common tie points of permanent topographic features and the dataset was processed as 12 standalone sub-datasets, rather than all processed together. Given the size of the monitored area, dividing the point cloud into smaller datasets avoids propagation of inaccuracy through large co-registered scan series. ICP (iterative closest point) algorithms (Besl and McKay, 1992), that minimize the distance

between two point clouds, were used to determine the best alignment of subsets surveyed at different time in order to obtain the best co-registration within a time series. The same procedure was applied between subset point clouds and a commercial airborne laser scanner derived point cloud (mean density: 6.9 pts/m^2) acquired in June 2009 to place the TLS data into the standard Lambert projection coordinate system used in France. The initial survey point cloud data was set as the surface model of reference. Each successive survey was georeferenced onto this reference using ICP. The topographic change occurring between two successive surveys are too localized to influence the global co-registration within two survey data subsets consisting of millions of data points, hence the alignment accuracy. More details about multiple scans registration techniques and point cloud time series comparison can be found in Oppikofer (2009). The generated surface produced by the above procedure has a point spacing ranging from 2.5 to 18 cm according to the distance of acquisition. A maximum range of about 800 m was reached on the top peak of the catchment with a point cloud density of 25 pts/m^2. The surface coverage of our surveys represents 84% of the deforested area under investigation (Table 2).

3.2 Topographic change identification and characterization

The active geomorphic features within two successive datasets were identified on a point by point basis using the short distance neighbouring point search algorithm (Bitelli et al., 2004) that computes in 3-D the shortest difference vectors between the points of two datasets. The vector sign indicates the net change direction of topography, i.e. surface of erosion or deposition. A set of points (cluster) was considered as active if at least 8 adjacent points of similar sign displayed an absolute difference above the limit of detection (LoD, see Section 3.4). Each active feature was outlined visually using the point cloud of difference (Fig. 5a). The point clusters of both survey datasets, which correspond to the topography of the active features, were extracted according to their spatial extend coordinates and each detected geomorphic feature was labelled as follows:

(1) Rock slope erosion, characterised by rockfall/-slides;

(2) Hillslope erosion, specifically the reworking of loose/compacted debris on slope, in gullies and channels;

(3) Deposition, including material aggradation initiated by both rock slope failure (new production) and remobilisation of debris.

Using the images captured by the TLS integrated camera, clusters of points not corresponding to geomorphic process activity, such as snow melt, were ignored.

3.3 Volume computation of each geomorphic feature

As the volume of active features cannot be directly computed by differencing TLS point datasets, the active features of two successive point clouds must be interpolated into continuous surfaces (DEM). Gridded model (or raster) is regarded as being the most effective type of model to use for irregularly distributed datasets which sometimes contain few or no points (El-Sheimy et al., 2005), as can be the case for rockfall and erosion scars. The algorithm chosen for interpolation of the DEM has little influence on the final result, as TLS data provide an extremely dense coverage of the detected objects (Anderson et al., 2005). So, they were interpolated using linear inverse distance weighting (Burrough and McDonnell, 1998) and generated in a regular grid separately. Grid spacing and direction of interpolation were designed in a specific way for each feature: the coordinate system of reference was replaced by a local orthogonal system where the x-y axes represent the average plane of topography nearby (Fig. 5b). This new reference frame was defined using eigen-value decomposition of the covariance matrix of the point cloud of reference (Shaw, 2003). Interpolating the surface elevation in the direction of local topography allows the generation of a realistic DEM independent of slope steepness and thus, a close realistic representation of topography in the case of overhanging features. The cell size was defined according to the point spacing distribution of both datasets. A series of tests revealed that setting the grid spacing at 68 % of the cumulative frequency distribution of point spacing provides a continuous surface reconstruction while keeping a high degree of detail from the point cloud. This ensures an accurate volume computation of geomorphic features. The volume was computed as the sum of the cell difference in elevation (both positive and negative) between the successive DEM. Absolute cell differences lying below a given threshold (see section 3.4) were not considered. This volume computation using local deterministic method of interpolation and an adaptive gridding approach was developed in the Matlab numerical computing environment.

3.4 Point cloud accuracy and limits of detection of the geomorphic features

A reliable identification of erosion and deposition features requires the definition of a LoD, where the change of elevation between successive point clouds can be considered as real as

opposed to noise. Each TLS data point has theoretically a unique precision depending on the range and laser incidence angle (Buckley et al., 2008). In practice, the individual point precision of a scan can be assumed to model a surface with a global uniform uncertainty, considering the very high point density (Abellan et al., 2009). Given the homogeneity of surface error, and considering that the distance between sequential points at a position (x,y) should tend to zero, the accuracy of TLS data can be estimated by substituting the precision of each data point by a singular measurement of the error associated with the entire point distribution across the surface (Lane et al., 2003). Hence, the uncertainty related to both scans registration and point cloud georeferencing, the instrumental error included, was defined by the standard deviation of the distance (σ_d) between the points (Fig. 6). The LoD was therefore set at 2σ of the co-georeferencing and corresponds to the 95 % confidence limit (Table 3). Comparison with the approach considering the error propagation for all uncertainties associated with each point cloud, and assuming a normal distribution of the error in distance (Taylor, 1997), shows that the uncertainties considered here are consistent.

In the case of volume computation, information on elevation uncertainty associated with each point cloud survey needs to be extended to the DEM on a cell by cell basis. For any grid cell (i,j) generated by the interpolation of adjacent points *p* with independent elevation, the uncertainty of a cell elevation can be considered as the standard deviation (σ_e) of the data points elevation, where $\sigma_{\bar{e}_{i,j}} = \sigma_{e_p} / \sqrt{n}$ according to the equation of standard error of the mean, *n* being the number of points to define the cell elevation. The elevation uncertainty for each cell in a DEM of difference is then expressed by:

$$\sigma_{\Delta\bar{e}_{i,j}} = \sqrt{\left(\sigma_{1\bar{e}_{i,j}}\right)^2 + \left(\sigma_{2\bar{e}_{i,j}}\right)^2} \,. \quad (1)$$

The volume uncertainty is then calculated by summing up the derived volume uncertainty of each cell of the feature as follow:

$$\Delta\bar{v}_{feature} = a\left[\sqrt{\sum_{i=1}^{n}\sum_{j=1}^{n}\left(\sigma_{\Delta\bar{e}_{i,j}}\right)^2}\right], \text{ with } a = \text{cell area.} \quad (2)$$

The smallest detectable volume is about 10^{-3} m^3 (10 x 10 x 10 cm) (Table 3), but can reach up to 0.006 m^3 (25 x 25 x 10 cm) depending on the point spacing at maximum range. Topographic change detection and volume computation accuracy depend not only on the quality of the TLS data, such as point density and post-processing related inaccuracy. It also

depends on the complexity of the surface geometry, like in our case, by integrating the range in position of all data points defining each grid cell value of a feature. Monitoring the hillslope activity is also limited by the ability of the process to create a distinct topographic change. Consequently, the deposition of individual small rockfalls was not always detected, as detached rock masses fragment into smaller pieces that are below the LoD. A similar issue was observed for erosion processes within debris. Nevertheless, most of the material accumulation could be related to upslope landslides or scouring. The sediment budgets were therefore kept in volumetric units, as they are commensurate for a consistent analysis. They were not converted to mass, although this would make more sense for comparing hillslope processes and rock slope yields. Such conversion requires an accurate density value of each surface process, whose approximations introduce additional unknowns. Deposition related to rock failures may therefore be slightly overrepresented in the sediment balance, although this could be partly compensated for by a limited detection of small features.

3.5 Sediment budgets of the Manival torrent

Monitoring of the coarse sediment transfer has been performed all along the main torrent channel to the sediment trap located downstream on the alluvial fan. The in-channel storage change was established after every noticeable flow event, using the morphological approach based on cross-section survey techniques (Ashore and Church, 1998), and the volume of sediment deposited in the sediment trap was measured by TLS survey differencing. Sequential volumes of recharge enable to study the influence of debris supply from the production zone through the seasons. The characteristics and observational analysis of this event-based monitoring was documented in details in Theule et al. (2012, 2015) and is therefore not described any further.

3.6 Estimation of debris production rate

A rate of debris production for the study period is obtained from the total volume of rock slope erosion. An objective estimation can be deduced by characterising the cumulative distribution of rockfall volumes with a power law as follows (Gardner, 1970):

$$N(v > V) = aV^{-b}. \quad (3)$$

N is the rockfall frequency for a volume v greater than V, a and b are constants. a depends on the study size and on rock slope properties, whereas b tends to be rather site independent

(Dussauge-Peisser et al., 2002; Dewez et al., 2011). Considering that rock slope process activity causing rockfall does not fluctuate much over time, the inventory analysis can be used to infer the frequency of occurrence of larger events. This is done by integrating the rockfall frequency derivative $n(v) = \frac{dN}{dV}$ over the range of potential volumes. Estimation of the total volume V_t per unit time that can be expected in average over a longer period of observation is therefore expressed by (modified from Hantz et al. (2002)):

$$V_t = \int_{n(V_{min})}^{n(V_{max})} V dn = -ab \int_{V_{min}}^{V_{max}} V \times V^{-b-1} dV = -ab \int_{V_{min}}^{V_{max}} V^{-b} dV = \frac{-ab}{(1-b)} V^{1-b} \Big|_{V_{min}}^{V_{max}} . \quad (4)$$

The goodness of fit of the power law was evaluated with the χ^2 test (Taylor, 1997) and the standard deviation of value *a* and *b* were determined with the maximum likelihood estimate (Aki, 1965). The erosion rates are assessed by dividing V_t with the surface prone to rockfall.

4 Results: Hillslope process activity monitoring

4.1 1st monitoring period (April 2009 – August 2009)

The topographic changes recorded from July to August 2009 did not show any relevant geomorphic activity (only a few small rockfalls). These results were therefore merged with the preceding monitoring period.

Rock slope activity is dominated by individual small rockfalls distributed throughout the upper catchment. Only few events exceed 1 m^3, such that contributions in terms of debris production are marginal in most parts of the catchment (Fig. 7). The most significant geomorphic activity was located almost exclusively in the major gullies of Baure and Grosse Pierre ravines, and consists essentially of debris scouring of a few 100 m^3 re-deposited further down. Material re-entrainment was also observed in several other smaller gullies, but their volumes are relatively small. The rock couloirs of the Genievre subcatchment and the scar of the old rock deposit barely showed any geomorphic activity. The channels displayed a net incision (-636 m^3 ± 43) in the upper reaches. Bedload aggradation remains very low (+90 m^3 ± 6). Below the upper confluence, the channel trunk exhibits a mixed pattern of zones of erosion (-60 m^3 ± 2), such as gravel-wedge scouring, and zones of re-deposition of entrained material (+80 m^3 ± 4) induced by bedload transport.

4.2 2nd monitoring period (September 2009 – November 2009)

Rock slope activity remains similar in spatial extent and volumes to the previous survey period, but rockfall frequency is higher (Fig. 8). Hillslope process activity was more widespread on the east side, but more localized on the western valley walls, while the rock couloirs showed no geomorphic activity. In the upper headwater, material reworking was concentrated almost exclusively in the steep tributary gullies. They displayed scouring of a relatively large volume (-357 m^3 ± 12). Deposition features along the thalweg were almost inexistent (+18 m^3 ± 1.3). In the south-east, not only the Baure Ravine (net erosion: -61 m^3 ± 8), but the whole series of hillside gullies exhibited signs of activity, such as erosional segments alternating with deposition. On scree slopes, several minor areas with erosional rills and their associated debris deposits were observed, some of them reaching the channel trunk (+42 m^3 ± 2). Such small hillside debris flows were probably triggered by sediment entrainments within the rills, as no evidence of sliding at their head was observed. The channels show a net erosion upstream (-482 m^3 ± 18), whereas continuous incisions were more pronounced in the Manival channel (-443 m^3 ± 16) and also in the Roche Ravine (-40 m^3 ± 3). Deposition zones were almost completely absent (15 m^3 ± 1.3). Towards the upper confluence, the lower segments of Manival channel exhibited continuous zones of aggradation (97 m^3 ± 6) that were scoured on one side. This morphology is characteristic of closed-process debris flow levees and run-up zones beside the incised channel bed. Below the upper confluence, channel bed cut (-40 m^3 ± 2) and fill (+16 m^3 ± 1) was sparse and concentrated at the junction with hillside gullies. Such a pattern of bed reworking demonstrates the connectivity of the Baure gully series with the channel trunk.

4.3 3rd monitoring period (November 2009 – July 2010)

This period showed an important increase of rock slope erosion, both in frequency and magnitude, resulting from the occurrence of large slope failures and enhanced localized rockfall activity, for instance in rock walls made of calcareous marl situated directly above the Manival (2035 m^3 ± 39) and the Roche Ravine (256 m^3 ± 17) channels (Fig. 9). Most of debris collapses supplied the channel directly; the rest was temporary deposited in breaks in slope. The lower headwater part showed a great fluctuation as well (Genievre: 116 m^3; Grosse Pierre: 145 m^3). At the top of the Baure Ravine, 816 m^3 ± 25 of rock fragments contributed substantially to recharge the sediment storage at gully head. Below, debris infilling was continuously scoured. A 1170 m^3 ± 18 rockslide is responsible for a large channel infill in the

Manival subcatchment. Several other smaller rockfalls contributed to the recharge of tributary gullies and scree hollows. In the Roche Ravine, debris deposits were sparse, because rockfall remained of low magnitude on average (571 events < 1 m^3), although frequency was high (578 events). The large debris infill at the channel head was caused by two erosion scars in the gullies (270 m^3 ± 14 and 65 m^3 ± 4). In the rock couloirs of the Genièvre subcatchment, a significant accumulation of material from landslides and rockfalls was observed (remnant volume: 204 m^3 ± 13), taking into account that the hillslope erosion represents 450 m^3 (± 14). In the Grosse Pierre Ravine, 343 m^3 ± 17 of debris were accumulated at the rock couloir outlet, recharging the scree slope above the channel head. In the Col du Baure, relatively large aggradation in the lower part of tributary gullies was observed (remnant volume: +142 m^3 ± 2), resulting from material entrainment. Several debris slides were also detected on scree slopes, without any contact with the channel trunk.

The upper channel-reaches were clearly depositional, as a consequence of large slope failures. The Manival channel showed a continuous zone of remnant accumulation of 948 m^3 (± 18) of which a portion was carried along downstream as bedload. Towards the confluence, erosion dominated (-487 m^3 ± 19) over deposition (+25 m^3 ± 3). In the Roche Ravine, a continuous zone of erosion in the scar of the old rock deposit produced debris accumulation mostly on the slope. But a landslide of 190 m^3 ± 9 reached the channel. Overall, aggradation was observed all along the channel head (+148 m^3 ± 18) and scouring was limited (-65 m^3 ± 4). From the confluence downstream, the channel behaviour is dominantly erosional (-97 m^3 ± 4) almost without any aggradation (+3 ± 0.3 m^3).

4.4 Rock slope production inventory

Over the 16 months, 1,866 rockfalls with volumes ranging from 10^{-4} to 10^3 were recorded. This yields a total of 3,575 m^3 ± 30 and an erosion rate of 3.1 mm/yr, given the topographic surface area of rock faces. The inventory follows a power law (Fig. 10) with a 99 % confidence level for events larger than 3 m^3 (χ^2 value = 17.3). For events larger than 1 m^3, the power law is accepted at the 95 % confidence level (χ^2 value = 5.89). Both threshold volumes provide a b-value close to 0.81 ± 0.06. Considering only the volumes above 10 m^3 (25 events) gives a b-value of 0.76. Below 0.1 m^3, the observed frequency deviated clearly from power law regime until the roll-over reaches an approximately constant rate for the smallest volumes. According to our inventory, rockfall of more than 1 m^3 are expected 153 ±

11 times per year on average. The largest event (1,170 m^3) occurs every two years, and the one year return period rockfall has a volume of approximately 465 m^3. Considering only these classes of volumes of the inventory (see Table 6), the rock slope production reaches a rate of 3,678 m^3/yr ± 210 (4 mm/yr ± 0.3).

4.5 Torrent in-channel storage changes

Two debris flows with multiple surges and several remarkable bedload transport events were observed in the main torrent during the survey period (Theule et al., 2012). A debris flow occurred on the 25th August 2009, caused by a short duration rainstorm. The volume of sediment eroded in the torrent (5,232 m^3 ± 136) is equivalent to the volume that was re-deposited in both the torrent itself and the sediment trap (5,072 m^3 ± 125), suggesting that the majority of entrained material was stored in the torrent (Table 4). Sediment input from the headwater can be considered as marginal. Before that, no significant torrent activity was observed, despite a series of rainfall events with low to moderate intensity. In September 2009, a long period of moderate rainfall intensity caused material reworking by bedload transport all along the torrent. However, no sediment was supplied to the sediment trap. A net gain of storage in the headwater was therefore inferred. In October, a succession of low intensity rainfall events triggered sediment transport in the torrent that accumulated in the sediment trap with a volume of at least 302 m^3 ± 36. The sediment budget indicates clearly a recharge of 229 m^3 ± 31, a transfer of debris that was stored mostly in the distal part of the torrent. Throughout the winter, a gradual incision was observed all along the torrent resulting from frequent periods of low intensity rainfall as well as snowmelt. Due to maintenance (dredging), the sediment trap was disturbed and no reliable data was available. No sign of significant sediment activity was detected anyway. A new debris flow on June 6th deposited 3,320 m^3 ± 176 in the sediment trap. This time, a certain supply of sediment from the headwater was observed (~ 270 m^3). This event was followed by series of intense rainfall events without much reworking in the distal part, suggesting that any significant transfer occurred into the torrent downstream. The in-torrent storage changes and estimated recharge budgets are shown for each monitoring period in Figure 11.

5 Synthesis

The overall transfer dynamics, from debris source zone to the apex of the fan, is illustrated in Figure 12. The volumes detected during the 16-month study period reveal a net export of 3,378 m^3 ± 361 of sediment from the headwater to the main torrent (Table 5). The overall rock slope yield is 3,575 m^3 ± 30, for a volume of erosion reaching 3,129 m^3 ± 150 on the hillside and 1,809 m^3 ± 92 in the channel complex. Volume of deposition, induced from both debris production and material reworking, yields a total volume of 5,135 m^3 ± 251, of which only 1,382 m^3 ± 56 (27 %) is linked to the channel complex. In the main torrent, the sediment transfer was relatively large (~20,000 m^3; net storage change -4950 m^3 ± 118) and essentially related to the occurrence of two debris flows (Theule et al., 2012), depleting significantly the in-torrent sediment storage of the distal parts (entrainment zone). Material deposited in the sediment trap for the survey period yields 6075 m^3 ± 45. During the autumn, bedload transport of hundreds of m^3 contributed to sediment recharge throughout the torrent.

In the spring-midsummer period, the hillside sediment budget yields a total rock slope production of 99 m^3 ± 6, for a volume of erosion of -547 m^3 ± 50 and deposition of +408 m^3 ± 35 (Table 5). This suggests that about 238 m^3 ± 61 of material was supplied the channel complex, originating almost exclusively from material re-entrainment in gullies (Fig. 13). The sediment budget of the channels indicates a significant reduction in storage (-487 m^3 ± 44), comprising large and continuous incisions (-636 m^3 ± 43) in the upper reaches and material aggradation (+149 m^3 ± 11) in the lower reaches resulting mostly from zones of transient re-deposition. This results a recharge of the torrent of +726 m^3 ± 103 for this survey period.

During the late summer - autumn season, the total volume of hillside erosion is of -640 m^3 ± 27, due to a widespread scouring of the tributary gullies located east and southeast of the headwater (Fig. 14). The total volume of rock slope production (50 m^3 ± 3) and deposition (+182 m^3 ± 12) remained low. Overall, the sediment budget indicates, that the hillslope contributed about 510 m^3 ± 30 of sediment to the channel reaches (Table 5). The sediment budget of the channels yields -522 m^3 ± 20 of erosion for +127 m^3 ± 13 of deposition. This is characterized by bedload reworking in both low-order and trunk channels, and a progressive transfer of +904 m^3 ± 51 of material into the torrent.

During winter - spring 2010, a total deposition volume of +3,163 m^3 ± 147 is recorded on the hillside, for an eroded volume of -3,129 m^3 ± 150. A relatively large production of debris (3,424 m^3 ± 89) is observed (Table 5). The net sediment balance on the hillside yields to a

supply of +2,203 m^3 ± 187 of sediment into the channels, and the net sediment balance for the channel complex indicates an increase of in-channel sediment storage of +455 m^3 ± 47, for a total volume of deposition of 1105 m^3 ± 36 and erosion of 651 m^3 ± 29 due to large portions of bed scouring in the downstream reaches. Sediment transfer into the torrent is 1749 m^3 ± 199 (Fig. 15).

6 Discussion

6.1 Debris supply through rock slope production

Debris production from rock walls shows a strong seasonal pattern. The great majority of recorded rock instabilities in both magnitude (95%) and frequency (75%) occurred during the cold period. Previous studies of the calcareous cliffs near Grenoble, which have a similar morphotectonic context, revealed that freeze-thaw cycles are the main triggering factor of rockfall (Frayssines et al., 2006). Ice jacking can cause microcrack propagation leading to failure (Matsuoka and Sakai, 1999). Along the eastern ridge, the bedrock surface is often highly fractured, suggesting frost shattering. The spatial pattern of rockfall strongly suggests also a tectonic-lithological influence that can be explained by differential erosion between the successive limestone and marl beds. In the rock wall series on the west side, the monoclinal configuration of the bedding, combined with a strong difference of competency between stratigraphic sequences, give rise to overhanging formation highly susceptible to failure. On the east side, the bedding is mostly cataclinal and approaches dip-slope, depending on the slope. Rock failures initiated by planar sliding on bedding planes were observed.

The observed debris production follows a power law distribution in a range covering at least 3 orders of magnitude [10^0-10^3]. The exponent b is slightly higher than the average value reported for the Grenoble cliffs [0.4-0.7] (Hantz et al., 2011), but is in agreement with other short inventories covering a lower range of volume [10^{-2}-10^2] (Hungr et al., 1999; Dussauge et al., 2003). Inventories dominated by small volumes tend to increase the b-value, compared to the ones covering rather large volumes (Stark and Hovius, 2001). Above 100 m^3, the deviation from the power law may be attributed to the short period of sampling for events of such large magnitude. The roll-over encountered towards small volumes results most likely in the under-detection of the number of events. This sampling bias being far above the minimum volume of detection (0.006 m^3), therefore another behaviour characterizing the failure of

small volumes cannot be excluded. This may take the form of a physical erosion process that differs from the one influencing larger instabilities, which are controlled primarily by the geometrical and geomechanical properties of the rock mass (Selby, 1993; Sauchyn et al., 1998), and tectonic weakening (Cruden, 2003; Coe and Harp, 2007). As observed here, low magnitude rockfall events represent a low proportion of overall debris supply, even though they vary locally from 1 or 2 orders of magnitude in volume over time. The total amount of sediment available is only significantly influenced by high magnitude instabilities (Fig. 16).

Previous sediment budgets derived from topographic measurement using stereophoto-grammetry estimated the highest erosion rates over an average of 40 years to range from 10.8 mm/yr to 17.8 mm/yr in the headwater (Veyrat-Charvillon and Memier, 2006). Given the large uncertainty of the approach, and the fact that they measured the hillslope and thalweg geomorphic activity, these values are broadly consistent with the erosion rate derived here from a short period rockfall inventory, by assuming the possible occurrence of rockslide magnitudes [10^6-10^7]. Considering that the power law is valid for larger slope failures, a 7,500 m^3 event can be expected every 10 years, and a 120,000 m^3 event every 100 years. The average debris production ranges between 5,587 ± 241 to 12,903 ± 305 m^3/yr, assuming a maximum potential erosion of 10^5 and 10^7 m^3 respectively, over several centuries (Table 6). No historical Manival rockslide exists to support this estimation. The large old rock deposit (~6.1 Mm^3) of the upper catchment is the largest detected event, but it may have formed from several rock collapses. Rockfall inventory of the Grenoble cliffs reports volumes smaller than 10^5 m^3 for the last century, and 10^7 m^3 since the 17th century (Hantz et al., 2003]. Such a magnitude is also likely at the Manival. A mean rate of rock slope erosion of approximatively 10 mm/yr. (10,000 m^3/yr) can be therefore expected in the upper catchment over the century.

Upstream from the Manival channel, scouring of debris slopes and scree hollows triggered by rock slope production accounted for about 40% of the net erosion recorded during the autumn period, and 25% in the Baure Ravine over the entire study period. The spatial pattern of geomorphic work showed, that hillslope process activity was observed principally in gullies and scree slopes situated directly below active rock walls. The dominant mode of debris supply in the Manival headwater is therefore highly episodic, implying a great spatial heterogeneity in sediment recharge rates.

6.2 Debris supply through hillslope activity

As rock slope activity was very limited from spring to autumn, hillslope geomorphic activity dominated sediment recharge during this period. Until the end of August, hillside gullies and low-order channels remain almost inactive in terms of sediment delivery. Conversely, the autumn period was characterized by a general increase in the intensity of geomorphic activity. Continuous scouring and the relative paucity of deposition features from hillside gullies as well as clear incisions and micro debris flows in channel reaches indicate that mobilized material was almost entirely entrained downstream by runoff. For the entire area, the hillside contribution represents on average a volume 5 times larger than the volume that was observed in spring and summer, and channel bed reworking was of much larger magnitude as well.

During winter-spring 2010, the total volume of deposition recorded on the hillside significantly exceeds the rate of deposition recorded so far, resulting from the huge increase of debris production that can be attributed to the winter according to observations carried out in the preceding spring. Hillslope and gully erosion remain on average comparable to the volumetric transfer of sediment observed in the preceding autumn, implying a clear connectivity.

These negative sediment balances in all sediment cascade components suggests a very high degree of connectivity between hillside and channels in autumn, and hillside fan deposits observed in early-spring along low-order channel banks reflect an effective hillslope-channel coupling. This differs from effective sediment transfer occurring mostly during the summer (e.g. Berger et al, 2011; Cavalli et al, 2013).

6.3 Sediment recharge of the torrent

The sediment input, back-calculated from the in-torrent storage changes, is consistent with the net sediment output recorded from the headwater for the first two survey periods. In the torrent, the morphological monitoring that started in July revealed almost no sediment recharge (< 70 m^3) and is coherent with observations made in the summer in the upper catchment. The headwater sediment output must have accumulated before, probably mobilized as bedload by common runoff events in spring. In autumn, both budgets are approximately equal (1018 ± 84 m^3 against 904 m^3 ± 51), considering that few segments between both entities are missing, and that both budgets were in volumetric units, despite having different sediment densities. The morphological budget indicates that the torrent

experienced a net recharge in the distal part, and emphasizes the clear connectivity from the production zones to the torrent, as mentioned before. In the 3rd survey period, the headwater sediment balance indicates a net export of debris (1749 m^3 ± 199), whereas the morphological monitoring detected no significant volumes of debris entering the main torrent. Even the recharge (sediment input, Fig.11) measured during the June debris flow events (< 600 m^3) remains far below the transfer of sediment recorded upstream in the headwater. This discrepancy may result from material deposition occurring in the non-monitored segments at the headwater outlet. But field studies did not confirm this. The analysis of past series of sediment budgets performed in the upper Manival catchment (Veyrat-Charvillon, 2005) reveals, that the spring-early summer time currently exhibits a period of recharge following a phase of discharge within a short time lapse depending on the hydrometeorological and snow melt conditions. The most reasonable explanation is therefore the relatively long time interval between measurements, such as the successive reworking of bedload transport suppressing the cut and fill pattern, and masking the short term behaviour of sediment transfer in the torrent. This is a well-known issue when working with channelized hillslope processes (Fuller et al., 2010). Although this monitoring aspect concerns the topographic changes recorded by TLS in the headwater as well, geomorphic activity, such as micro debris flows and continuous channel bed degradation, strongly suggests phases of sediment recharge preceding the debris flow events, which would be consistent with other studies (e.g. Brayshaw & Hassan, 2009; Marchi et al., 2002, Bennett et al., 2012).

6.4 Possible causes of seasonal fluctuations in debris supply

The Manival headwater experienced low geomorphic activity through the summer, and consequently low sediment recharge of the torrent, even though rainstorms were of sufficiently high intensity to trigger debris flows of significant magnitude in torrent. Considerations of the temporal pattern of sediment transfer and the analysis of erosion features, like alternating areas of scouring and infilling in gullies, suggest that runoff still exerts an important role on the headwater sediment dynamics. A clear relation between sediment transfer magnitude and precipitation remains complex however (Fig. 3), as often the case in mountainous catchments (VanSteijn, 1996; Bovis and Jakob, 1999; Pelfini and Santilli, 2008). The enhanced geomorphic activity observed in the hillside of several headwater subsystems, for instance during the autumn period, induced a simultaneous yet highly heterogeneous response in their channel reaches. A significant increase of bed incision

and debris flow similar reworking was observed in the upper reaches of the Manival subcatchment, implying an important sediment transfer. In contrast, the activity of other channel reaches was reduced by half, e.g. in Roche Ravine, or even remained geomorphically much less active with only little sediment recharge.

Considering that meteorological conditions were similar, this opposite behaviour may only be explained by a certain depletion of debris availability. This reduction of sediment yield can come not only within a supply-limited regime of the contributing area (Jakob et al., 2005; Glade, 2005), but also from the fact that check dams, like bedrock dominated reaches, inhibit channel bed incision. Hence, the sediment storage has to be refilled either from the contributing hillside or from upstream mass movement. A similar observation can be drawn from the Grosse Pierre Ravine sediment budget, whose gully downslope remained completely disconnected from the head of the subcatchment over the whole study period at least. Although this ravine is very steep and incises the large old rock deposits, no geomorphic work was observed, resulting most likely from the absence of debris supply from upstream. Hillside sediment delivery seems therefore to be clearly a limiting factor to sediment yield from low to high-order channels, and thus to the sediment recharge rate of the debris flow torrent downstream. As the occurrence of bedload transport and micro debris flows is controlled predominantly by the availability of sediment, even very intense rainstorm derived runoff does not automatically lead to significant transfer of sediment from the hillside to low-order channels in the case of material depletion.

But still, this behaviour is somehow equivocal, considering the fact that the transport capacity of ephemeral stream runoff and sheetwash related to high intensity rainstorms are larger than the one generated by low intensity long duration rainfall; above all, when gully material (like in the Manival) can be characterized as coarse and poorly sorted rockfall fragment derived debris. Lenzi et al. (2003) interpreted the annual fluctuation in sediment yield as the effect of sediment source destabilization or reactivation following a high-magnitude flow event, which facilitates material entrainment by subsequent runoff. Johnson and Warburton (2006) refer to the influence of sediment source characteristic in the control of hillslope sediment discharge. The explanation may be, that the 25th August rainstorm dramatically altered the debris sources in a way that the autumn rainfalls, although of lower intensity but longer flood time, were able to transfer sediment downslope, for instance by saturating debris deposits in the long term. Excess pore-fluid pressure in debris deposits can persist for days to weeks after sediment

emplacement (Major and Iverson, 1999; Major 2000), making debris deposits geotechnically less stable.

Although depending on the local geomorphological setting, such as slope gradient, local topographic hollow, degree of convergence (Reneau et al., 1990; Stock & Dietrich, 2006; Mao et al., 2009), these observations tend to show that long lasting rainfall reduces the stability of the coarse surface layer that armours the gullies and scree slopes. This in turn effects the amount of debris supply from the hillside, despite the flow capacity and sediment availability.

7 Conclusions

This investigation of a yearly pattern of sediment dynamics underlines that the seasonal cycle of sediment discharge from the headwater supplying the Manival torrent with debris consisted of two phases of recharge: one phase in early spring, linked to enhanced debris production and runoff conditions; a second phase in autumn, during long periods of rainfall. Furthermore, the occurrence of the debris flow events was made conditional on a net sediment delivery toward the torrent.

Overall, the torrent effectiveness seems to be controlled early in the year, from winter to spring, by sediment production and later in the year by the ability of hydrological effects to weaken the remnant debris sources, with debris availability being only one of the limiting factors at the Manival torrent. The rate of sediment delivery, directly recharging both hillside and low-order channels, is controlled by high magnitude slope failure of moderate frequency which occurred mostly during winter time. Consequently, material re-entrainment concentrates locally in specific tributary gullies. The delivery of sediment to the torrent may be related to the hydrometeorological conditions since the last rainstorm, rather than to flow capacity directly. Low-order reaches contribute significantly to the sediment delivery mechanism of the catchment headwater, by controlling storage and routing processes. Hence, the recharge threshold required for a new debris flow to occur at the Manival depends primarily on the short-term debris supply, partly derived from the rate of rock slope sediment production and partly derived from mobilizing debris on the hillside. The rate of sediment recharge in the torrent is however greatly intermittent, since production and entrainment are both highly stochastic processes. This regime of headwater sediment delivery may have been identified in other nearby mountain environments, but very little literature exists (Alvarez and

Garcia Ruiz, 2000; Veyrat-Charvillon, 2005; Berger et al., 2011), that has explored in sufficient detail the time scale of sediment discharge, e.g. on a seasonal basis.

Debris flow magnitudes have so far been mostly determined based on volume estimates derived from past events, reducing the susceptibility analysis to the known history. Monitoring of the in-storage changes within the torrent linked to the debris supply can help to improve knowledge on the recharge threshold leading to debris flow activity, and therefore their prediction. According to the rock slope production observed in this study, 10,000 m^3/yr of debris supplying the headwater channels can be expected in Manival over a century. Although the multiplicity of sediment sources and mode of transfer operating at different spatial and temporal scales, the pattern of processes governing the sediment dynamics can be considered precisely on a seasonal basis using TLS techniques. Therefore maximum sediment discharges from the torrent system can be specified. Without direct measurement of the rate of sediment flux and of the coupling between hillslope and channel processes, this cannot be rigorously determined. The timing of sediment budget monitoring is however a crucial aspect for their later interpretation.

Acknowledgements

The authors would like to thank their colleagues at IGAR and IRSTEA Grenoble (ex. CEMAGREF), in particular A. Pedrazzini and M.-H. Derron for their valuable comments during the preparation of this publication. This study was funded entirely by the University of Lausanne, except for the event-based cross-section surveys that was funded by the Pôle Grenoblois d'étude et de recherche pour la prévention des risques naturels. The ONF-RTM38 is acknowledged for making the access to the upper Manival Catchment easier.

References

Abellàn, A., Jaboyedoff, M., Oppikofer, T. and Vilaplana, J. M.: Detection of millimetric deformation using a terrestrial laser scanner: experience and application to a rockfall event. Nat. Hazards Earth Syst. Sci. 9:365-372, 2009.

Aki, K.: Maximum likelihood estimate of b in the formula logN=a-bM and its confidence limits, Bull. Earthquake Res. Institute, 43, 237-239, 1965.

Alvarez, B. and Garcia-Ruiz, J.: Variability of sediment yield from a high mountain catchment, central Spanish Pyrenees. Arctic, Antarctic and Alpine Research 32, 4:478-484, 2000.

Anderson, E.S., Thompson, J.A. and Austin, R.E.: LiDAR density and linear interpolator effects on elevation estimates. International Journal of Remote Sensing 26(18): 3889-3900, 2005.

Benda, L. and Dunne, T.: Stochastic forcing of sediment supply to channel networks from landsliding and debris flow. Water Resources Research 33(12): 2849 – 2863, 1997.

Berger, C., McArdell, B. and Schlunegger, F.: Sediment transfer patterns at the Illgraben catchment, Switzerland: Implication for the time scales of debris flow activities. Geomorphology 125:421-432, 2011.

Besl, P.J. and McKay, N.D.: A method for registration of 3-D shapes. IEEE Transactions on Pattern Analysis and Machine Intelligence 14(2) 239-256, 1992.

Brayshaw, D., and Hassan, M.A.: Debris flow initiation and sediment recharge in gullies. Geomorphology 109:122-131, 2009.

Bremer, M. and Sass, O.: Combining airborne and terrestrial laser scanning for quantifying erosion and deposition by a debris flow event. Geomorphology 138:49-60, 2011.

Bennett, G.L., Molnar, P., Eisenbeiss, H., McArdell, B.W., 2012. Erosional power in the Swiss Alps: characterizing slope failure at the head of the Illgraben. Earth Surface Processes and Landforms 37, 1627–1640. http://dx.doi.org/10.1002/esp. 3263.

Berti, M., Genevois, R., LaHusen, R., Simoni, A. and Tecca, P.R.: Debris flow monitoring in the acquabona watershed on the Dolomites (Italian alps). Original Research Article Physics

and Chemistry of the Earth, Part B: Hydrology, Oceans and Atmosphere, Vol. 25, Issue 9, p.707-715, 2000.

Bitelli, G., Dubbini, M. and Zanutta, A.: Terrestrial laser scanning and digital photogrammetry techniques to monitor landslide bodies, in: Proceedings of the XXth ISPRS Congress Geo-Imagery Bridging Continents, XXXV, part B5, Istanbul, Turkey, 12–23 July 2004, ISPRS, 246–251, 2004.

Bovis, M.J. and Jakob, M.: The role of debris supply conditions in predicting debris flow activity. Earth surface processes and Landforms, 24: 1039 – 1054, 1999.

Brochot, S., Coeur, D., Lang, M. and Naulet, R.: Historique - Isère et torrents affluents. Utilisation de l'information historique pour une meilleur définition du risque d'inondation (rapport), Cemagref / Achtys, Lyon - Grenoble, 248 pp., 2000.

Brodu, N. and Lague, D.: 3D terrestrial lidar data classification of complex natural scenes using a multi-scale dimensionality criterion: Applications in geomorphology. ISPRS Journal of Photogrammetry and Remote Sensing 68, 121-134, 2012.

Buckley, S., Howell, J., Enge, H.. and Kurz T. : Terrestrial laser scanning in geology: data acquisition processing and accuracy considerations. Journal of the Geological Society 165: 625–638, 2008.

Burrough, P. and McDonnell, R.: Principals of Geographic Information Systems. Oxford University Press. 333 p., Oxford, 1998.

Cannon, S.H., Gartner, J.E., Parret, C. and Parise M. : Wildfire-related debris flow generation through episodic progressive sediment-bulking process, western USA. In: Debris-flow hazard mitigation: Mechanics, Prediction, and Assessment, Rickenmann D. and L. Chen (Eds.), Millpress, Rotterdam, p. 71-82, 2003.

Chandler, J.H. and Brunsden, D.: Steady state behaviour of the Black Ven mudslide : the application of archival analytical photogrammetry to studies of landform change. Earth Surf. Process. Landforms 20, 255-275, 1995.

Charollais, J., Dondey, D., Ginet, C., Lombard, A., Muller, J.P., Rosset, J. and Ruchat, C. : Carte géol. France (1/50.000°), Feuille Domène (33-34), Orléans, B.R.G.M, 1986.

Coe, J.A., Whitney, J.W. and Harrington, C.D.: Photogrammetric analysis of Quaternary hillslope erosion at Yucca Mountain, Nevada. Geol. Soc. Am. Astr. Progr. 25, 22, 1993.

Coe, J.A. and Harp, E.L. : Influence of tectonic folding on rockfall susceptibility, American Fork Canyon, Utah, USA. Nat. Hazards Earth Syst. Sci. 7:1-14, 2007.

Cruden, D.M.: The shapes of cold, high mountains in sedimentary rocks. Geomorphology 55: 249-261, 2003.

Decaulne, A. and Saemundsson, P.: Spatial and temporal diversity for debris-flow meterotological control in subarctic oceanic periglacial environments in Iceland. Earth surf. process. and Landforms 32:1971-1983, 2007.

Dewez, T. and Rohmer , J.: Probabilistic rockfall hazard: empirical computation based on ground-based lidar observations in Mesnil-Val, Normandy. Journée Aléa Gravitaires, 7-8 Septembre 2011, Strasbourg, France, p. 104-115, 2011.

Dietrich, W.F. and Dunne, T. :, Sediment budget for a small catchment in mountainous terrain. Zeitschrift für Geomorphologie Suppl. Bd. 29:191-206, 1978.

Dussauge-Peisser, C., Helmstetter, A., Grasso, J.-R., Hantz, D. , Jeannin, M. and Giraud, A.: Probabilistic approach to rock fall hazard assessment: potential of historical data analysis. Nat. Hazards Earth Syst. Sci., 2, 1-13, 2002.

Dussauge, C., Grasso, J.-R. and Helmstetter, A.: Statistical Analysis of Rock Fall Volume Distributions: Implications for Rock Fall Dynamics. J. Geophys. Res.-Sol. Ea., 108, 2-11, 2003.

El-Sheimy, N., Valeo, C. and Habib, A.: Digital terrain modeling: acquisition, manipulation, and applications , Artech House: Boston, MA, 257 pp., 2005.

Frayssines, M. and Hantz, D.: Failure mechanisms and triggering factors in calcareous cliffs of the Subalpine Ranges (French Alps). Eng. Geol. 86: 256–270, 2006.

Fuller, I.C. and Marden, M.: Rapid channel response to variability in sediment supply: Cutting and filling of the Tarndale Fan, Waipaoa catchment, New Zealand. Marine Geology, Vol. 270 (1-4): 45-54, 2010.

Gardner, J.S.: Rockfall: a geomorphic process in high mountain terrain, The Albertan Geographer, 6, 15-20, 1970.

Gidon, M.: Géologie de la Chartreuse - Sentiers de la Chartreuse : Circuit de la Dent de Crolles, Association "A la découverte du Patrimoine de Chartreuse", publ. 1d, 1° éd., 20 p., 9 fig., www. Geol-alp.com (last access : 18.04.2014), 1991.

Glade, T.: Linking debris-flow hazard assessments with geomorphology. Geomorphology 66:189-213, 2005.

Gruffaz, F.: Torrent du Manival (Isère), Etude de basin et de la plage de dépôts torrentiels (rapport), RTM/ONF, Grenoble, 66 pp, 1997.

Guzzetti, F., Peruccacci, S., Rossi, M. and Stark, C.P.: The rainfall intensity–duration control of shallow landslides and debris flows: an update. Landslides 5:3–17, 2008.

Hantz, D., Dussauge-Peisser, C., Jeannin M. and Vengeon, J.-M.: Rock fall Hazard: from expert opinion to quantitative evaluation. Symposium "Geomorphology: from expert opinion to modeling (April 2002)", Strasbourg, France, 115-122,2002.

Hantz, D., Vengeon, J.-M. and Dussauge-Peisser, C.: An historical, geomechanical and probabilistic approach to rockfall hazard assessment. Nat. Hazards Earth Syst. Sci., 3:693-701, 2003.

Hantz, D.: Quantitative assessment of diffuse rock fall hazard along a cliff foot. Nat. Hazards Earth Syst. Sci., 11: 1303-1309, 2011.

Hooke, J.: Coarse sediment connectivity in river channel systems: a conceptual framework and methodology. Geomorphology 56:79–94, 2003.

Hungr, O., Evans, S.G. and Hazzard, J.: Magnitude and frequency of rockfalls along the main transportation corridors of southwestern British Columbia, Canadian Geotechnical Journal, 36, 224-238, 1999.

Hungr, O., McDougall, S. and Bovis, M.: Entrainment of material by debris flows. Chapt. 7 (p.135-158) in Jakob M. & Hungr O. (Eds.), Debris Flow Hazards and Related Phenomena. Springer Verlag, Heidelberg, Germany, in association with Praxis Publishing Ltd, 2005.

Hungr, O.: Characterizing debris flows for design of hazard mitigation . In: Genevois R., D.L. Hamilton, and A. Prestininzi (Eds.), Proceedings of the 5th International Conference on Debris Flow Hazards Mitigation/Mechanics, Prediction, and Assessment, Padua, Italy. Italian Journal of Engineering Geology and Environment, Book of abstracts, Keynote lecture, p. 5,DOI: 10.4408/IJEGE.2011-03.B-001, 2011.

Jaboyedoff, M., Oppikofer, T., Abellan, A., Derron, M.H., Loye, A., Metzger R. and Pedrazzini, A.: Use of lidar in landslide investigations: a review. Nat Hazards 61:5-28, 2012.

Jakob, M., Bovis, M. and Oden, M.: The significance of channel recharge rates for estimating debris-flow magnitude and frequency, Earth Surface Processes and Landforms, 30: 755 – 766, 2005.

Johnson, R.M. and Warburton, J.: Variability in sediment supply, transfer and deposition in an upland torrent system: Iron Crag, northern England. Earth Surface Processes and Landforms, 31, 844-861, 2006.

Johnson, R.M., Warburton, J., Mills, A.J. and Winter C.: Evaluating the significance of event and post-event sediment dynamics in a first order tributary using multiple sediment budgets. Geogr. Ann., 92 A (2): 189–209, 2010.

Lane, S.N., Westaway, R.M. and Murray Hicks, D.: Estimation of erosion and deposition volumes in a large, gravel-bed, braided river using sysnotpic remoe sensing. Earth surf. Proc. and landforms 28:249-271, 2003.

Lenzi, M.A., Mao, L. and Comiti F.: Interannual variation of suspended sediment load and sediment yield in an alpine catchment. Hyerological Sciences - Journal des sciences hydrologiques, 48(6), 899-915, DOI: 10.1623/hysj.48.6.899.51425, 2003.

Loye A., Jaboyedoff, M., Pedrazzini, A., Theule, J., Liébault, F., and Metzger, R.: Morphostructural analysis of an alpine debris flows catchment: implication for debris supply. In: Genevois, R., Hamilton, D.L., and Prestininzi, A., Eds.., Proceedings of the 5th International Conference on Debris Flow Hazards Mitigation/Mechanics, Prediction, and Assessment, Padua, Italy, June 7-11, 2011, Italian Journal of Engineering Geology and Environment, p.115 – 126, DOI: 10.4408/IJEGE.2011-03.B-014, 2011.

Loye A., Jaboyedoff, M., Pedrazzini, A., Theule, J., Liébault, F., and Metzger, R.: Influence of bedrock structures on the spatial pattern of erosional landforms in small alpine catchments. Earth surf. Proc. and landforms 37:1407-1423, 2012.

Loye A., 2013. Budgeting rockfall and modeling sediment delivery in torrent systems, PhD Thesis, University of Lausanne (448 pp.)

Marchi, L., Arattano, M., Deganutti, A.M., 2002. Ten years of debris-flow monitoring in the Moscardo Torrent (Italian Alps). Geomorphology 46, 1–17.

Major, J.J. and Iverson, R.M.: Debris-flow deposition -- effects of pore-fluid pressure and friction concentrated at flow margins. Geological Society of American Bulletin, 111:1424-1434, 1999.

Major, J.J.: Gravity-driven consolidation of slurries – implications for debris-flow deposition and deposit characteristics. Journal of Sedimentary Research, 70(1):64-83. doi:1073-130X/00/070-64/03.00, 2000.

Mao, L., Cavalli, M., Comiti, F., Marchi, L., Lenzi, M.A., and Aratto, M.: Sediment transfer processes in two Alpine catchments of contrasting morphological settings. Journal of Hydrology 364:88-98, 2009.

Oppikofer, T.: Detection, Analysis and monitoring of slope movements by high-resolution digital elevetion models. PhD Thesis, Inst. of Geomatics and Risk Analysis, University of Lausanne, Lausanne, 2009.

Matsuoka, N., Sakai, H.: Rockfall activity from an alpine cliff during thawing period. Geomorphology 28:309–328, 1999.

Peiry, J.L. : Les torrents de L'Arve: dynamique des sédiments et impact de l'aménagement des bassins versants sur l'activité torrentielle. Rev. Géog. Alpine, 78:25-58, 1990.

Perroy, R.L., Bookhagen, B., Asner, G.P., and Chadwick, O.A.: Comparison of gully erosion estimates using airborne and ground-based LiDAR on Santa Cruz Island, California. Geomorphology 118 (2010) 288-300 ; 2010.

Péteuil, C., Maraval, C., Bertrand, C. and Monier, G.: Torrent du Manival: Schéma d'aménagement et de gestion du basin versant contre les crues, techn. report (unpubl.). Office National des Forêts, Service de Restauration des terrains en Montagnes de l'Isère, Grenoble, France, 107 p., 2008.

Reneau, S.L., Dietrich, W.E., Donohue, D.J., Jull, A.J.T. and Rubin, M.: Late Quaternary history of colluvial deposition and erosion in hollows, central California Coast Ranges. Geol. Soc. of Amer. Bull. 102:969-982, 1990.

Rickenmann, D.: Empirical relationship for Debris Flows, Nat. Hazards, 19:47–77, 1999.

Roering, J.J., Stimely, L.L., Mackey, G.H. and Schmidt, D.A.: Using DInSAR, airborne LIDAR and archival air photos to quantify landsliding and sediment transport, Geophysical Research Letters, 36, L19402, 5 p., doi: 10.1029/2009GL040374, 2009.

Sauchyn, D.J., Cruden, D.M. and Hu, X.Q.: Structural control of the morphometry of open rock basins, Kananaski region, Canadian Rocky Mountains, Geomorphology 22:313-324, 1998.

Shaw, P.J.A.: Multivariate statistics for the Environmental Sciences, Hodder-Arnold. ISBN 0-3408-0763-6, London, 2003.

Schlunegger, F., Badoux, A., McArdell, B.W., Gwerder, C., Schnydrig, D., Rieke-Zapp, D. and Molnar, P.: Limits of sediment transfer in an alpine debris-flow catchment, Illgraben, Switzerland. Quaternary Science reviews 28:1097–1105, 2009.

Selby, M.J.: Hillslope Material and Processes, Oxford Univ. Press, Oxford. 451 pp, 1993.

Smith, L.C., Alsdorf, D.E., Magilligan, F.J., Gomez, B., Mertes, L.A.K., Smith, N.D. and Garvin, J.B.: Estimation of erosion, deposition and net volumetric change caused by the 1996 Skeidararsandur Jökulhlaup, Iceland, from SAR interferometry. Water Resources Research 36(6): 1583-94, 2000.

Stark, C.P., and Hovius, N.: The characterization of landslide size distributions, Geophysical Research Letters 28:1091-1094, 2001.

Stock, J.D. and Dietrich, W.E.,: Erosion of steepland valleys by debris flows, Geological Society of America Bulletin, 118:1125 – 1148, 2006.

Taylor, J. R.: An introduction to error analysis, University science Books, Sausalito, California, 2nd Ed. , pp. 327, 1997.

Theule, J.I., Liébault, F., Loye, A., Laigle, D., Jaboyedoff,M., : Sediment budget monitoring of debris-flow and bedload transport in the Manival Torrent, SE France. Nat. Hazards Earth Syst. Sci. 12, 731–749, 2012.

Theule, J.I., Liébault, F., Laigle, D., Loye, A. and Jaboyedoff , M.: Channel scour and fill by debris flows and bedload transport, Geomorphology 243 92–105, 2015.

Van Steijn, H.: Debris-flow magnitude-frequency relationships for mountainous regions of Central and Northwest Europe. Geomorphology 15: 259 – 273, 1996.

Van Dine, D.F.: Debris flow and debris torrents in the Southern Canadian Cordillera. Can. Geotechn. 22: 44-68, 1985.

Veyrat-Charvillon, S. : Elaboration d'une méthode de prédiction du volume maximal d'une lave torrentielle (PREVENT), Doctor Thesis, Université Blaise Pascal Clermont-Ferrant 2, 354 p, 2005.

Veyrat-Charvillon, S. and Memier, M.: Stereophotogrammetry of archive data and topographic approaches to debris-flow torrent measurements: Calculation of channel-sediment states and a partial sediment budget for Manival torrent (Isère, France). Earth Surface Processes and Landforms, 31(2): 201 – 219, 2006.

Wu, Y. and Cheng, H.: Monitoring of gully erosion on the Loess Plateau of China using a global positioning system. Catena, 63, pp. 154-166, 2005.

Zimmermann, M., Mani, P. and Romang, H.: Magnitude–frequency aspects of alpine debris flows Eclogae Geol. Helv., 90, pp. 415–420, 1997.

Table 1. Dates of TLS acquisitions. Note that for the analysis, the 2nd survey was merged with the 1st one (see text for details).

Monitoring period	Start and end dates of Survey	Period ID
1st	01/04/2009 - 12/07/2009	MP1
2nd	12/07/2009 - 30/08/2009	merged with MP1
3rd	30/08/2009 - 11/11/2009	MP2
4th	11/11/2009 - 08/07/2010	MP3

Table 2. TLS data and surface coverage characteristics of the 5 subcatchments from MP1. As the view points and parameters of acquiring remained similar, the values are essentially the same for all surveys.

Subcatchment name	Surface[1]		Lidar Data Survey				Scanned area[1]	
	Total [km^2]	Vegetation cover [%]	Number of points	Mean spacing [m]	Mean range [m]	Mean density [pts/m^2]	Total [km^2]	[%] of the non-vegetated surface
Col du Baure	0.29	43.0	37,625,236	0.055	131	340	0.11	84
Roche Ravine	0.30	20.5	43,736,412	0.071	278	251	0.17	79
Manival	0.35	9.1	40,192,976	0.096	349	141	0.28	90
Grosse Pierre	0.08	9.0	9,703,449	0.110	447	145	0.07	97
Genievre	0.35	26.6	19,886,472	0.108	311	109	0.18	79
Production zone	1.36	22.7	151,144,545	0.081	275	219	0.82	84

[1] topographic surface area

Table 3. Registration and georeferencing standard deviations (in cm) of the position uncertainty on a point by point basis that was used to derive the LoD at 95% confidence interval and subsequently to detect topographic changes down to a certain minimum volume of geomorphic features.

Sub-catchment name	2σ co-registered [cm]				2σ co-georeferencing (LoD) [cm]			2σ Taylor uncertainty[(1)] [cm] $\left(\sigma_{d_{reg}} = \sqrt{\sigma^2_{d_{PC1}} + \sigma^2_{d_{PC2}}}\right)$		
	Survey				Monitoring period			Monitoring period		
	1st	2nd	3rd	4th	1st	2nd	3rd	1st	2nd	3rd
Col du Baure	1.9	1.7	1.5	1.5	5.9	6.9	6.9	5.1	4.5	4.2
Roche Ravine	3.2	2.9	2.6	2.7	8.4	9.4	9.0	8.6	7.7	7.5
Manival	4.6	4.1	3.0	3.4	9.6	10.2	12.2	12.3	10.2	9.1
Grosse Pierre	4.1	3.0	3.3	3.3	10.6	10.6	12.2	10.2	8.9	9.3
Genièvre	3.7	3.6	3.2	3.6	6.7	7.6	8.3	10.3	9.6	9.6

[(1)] *pc = point cloud used to generate the map (point cloud) of difference in 3D*

Table 4. Sediment budget (in m^3) of the Manival torrent established after noticeable events using the morphological approach after Theule et al. (2012). The torrent recharge (sediment input) is estimated from in-storage changes in channels and volumes deposited in the sediment trap (output).

Monitoring Period	Survey dates in the torrent	Sediment Output	Storage Change	Channel Erosion	Channel Deposition	Sediment Input	Total sediment Input
1st	#1 06/07/2009 - 28/08/2009	1873 ±62	-2034 ±559	5232±136	3199±63	0-63	0 - 63
2nd	#2 30 /08/2009 - 07/10/2009	0	789±84	1409±31	2197±53	736-842	934 - 1102
	#3 08/10/2009 - 12/11/2009	302±36	-73±66	1546±36	1473±31	198-260	
3rd	#4 13/11/2009 - 01/06/2010	580±45	-580 ±81	1961±45	1372±36	0-36	
	#5 02/06/2010 - 08/06/2010	3320±176	-3052 ±272	7658±178	4606±93	0-537	174 - 844(1)
	#6 09/06/2010 - 08/10/2010	819±46	-608 ±82	2246±46	1637±36	174-246	

(1) The TLS survey MP3 lasted until 08/07/2010; #6 were not considered for the analysis of the sediment budgets

Table 5. Overall headwater sediment budget recorded during the three survey periods and net sediment balance of the 16 months of monitoring (Sediment budgets for each catchment subsystem are detailed in the supplement).

1st monitoring period	Volume Total [m³]					
	Hillside		Channel		Headwater	
Rockfall	99.4	±5.9			99.4	±5.9
Deposition	408.2	±35.4	149.2	±10.9	557.4	±46.3
Erosion	547.2	±49.5	636.4	±43.3	1183.5	±92.8
Subtotal	-238.3	±61.2	-487.2	±44.7	-725.6	±103.9

2nd monitoring period	Volume Total [m³]					
	Hillside		Channel		Headwater	
Rockfall	50.5	±3.0			50.5	±3.0
Deposition	181.8	±12.2	127.2	±8.0	309.0	±20.5
Erosion	639.8	±27.1	522.5	±19.4	1162.3	±46.4
Subtotal	-508.5	±29.9	-395.3	±23.4	-903.7	±50.9

3rd monitoring period	Volume Total [m³]					
	Hillside		Channel		Headwater	
Rockfall	3424.9	±89.1			3424.9	±21.4
Deposition	3163.5	±147.9	1105.5	±36.4	4269.0	±175.6
Erosion	1941.6	±72.8	650.8	±28.8	2592.4	±91.6
Subtotal	-2203.0	±187.4	454.7	±46.5	-1748.3	±199.2

Total monitoring	Volume Total [m³]					
	Hillside		Channel		Total	
Rockfall	3574.7	±97.9			3574.7	±30.3
Deposition	3753.5	±195.6	1381.9	±55.6	5135.4	±251.3
Erosion	3128.5	±149.4	1809.7	±91.3	4938.2	±240.8
Subtotal	-2949.8	±264.9	-427.8	±106.9	-3377.6	±361.4

Table. 6: Rock slope debris production rate estimated from the inventory analysis using power law distribution of volume for potential rockfall (fig. 10).

Class of volume in m^3	10^{-3} – 10^{-2}	10^{-2} – 10^{-1}	10^{-1}- 1	1- 10	10^{1} - 10^{2}	10^{2} - 10^{3}	10^{3} - 10^{4}	10^{4} - 10^{5}	10^{5} - 10^{6}	10^{6} - 10^{7}
Measured frequency (per year)	143 (112.5)	742 (583.7)	789 (620.7	168 (132.2)	19 (14.95)	3 (2.36)	1 (0.79)			
Calculated frequency	36990 ±4366	5621 ±581	854 ±86	130 ±9.6	19.7 ±1.2	3.0 ±0.14	0.46 ±0.015	0.069 ±0.0013	0.011 $\pm 1 \cdot 10^{-4}$	0.0016 $\pm 1.2 \cdot 10^{-5}$
Cumulative Measured Frequency	1467	1355	772	152	19	3.1	0.79			
Cumulative Calculated Frequency	43619 ±5043	6629 ±677	1007 ±97	153 ±11	23 ±1.58	3.5 ±0.198	0.54 ±0.018	0.08 ±0.0014	0.01 $\pm 1.1 \cdot 10^{-4}$	0.0016 $\pm 1.2 \cdot 10^{-5}$
Fallen volume per year [m^3]	102 ±12	155 ±16	236 ±19	358 ±26	544 ±32	827 ±37	1257 ±39	1911 ±32	2904 ±8	4413 ±51
Total fallen volume per year [m^3]	298 ±43	454 ±59	689 ±79	1047 ±105	1592 ±136	2419 ±172	3676 ±210	5587 ±241	8491 ±249	12903 ±305
Cliff area	826804 m^2 (only the topographic rock slope surface)									
Erosion rate [mm]	0.36 ±0.05	0.54 ±0.07	0.83 ±0.1	1.3 ±0.1	1.9 ±0.2	2.9 ±0.2	4 ±0.3	6.8 ±0.3	10.2 ±0.3	15.6 ±0.4

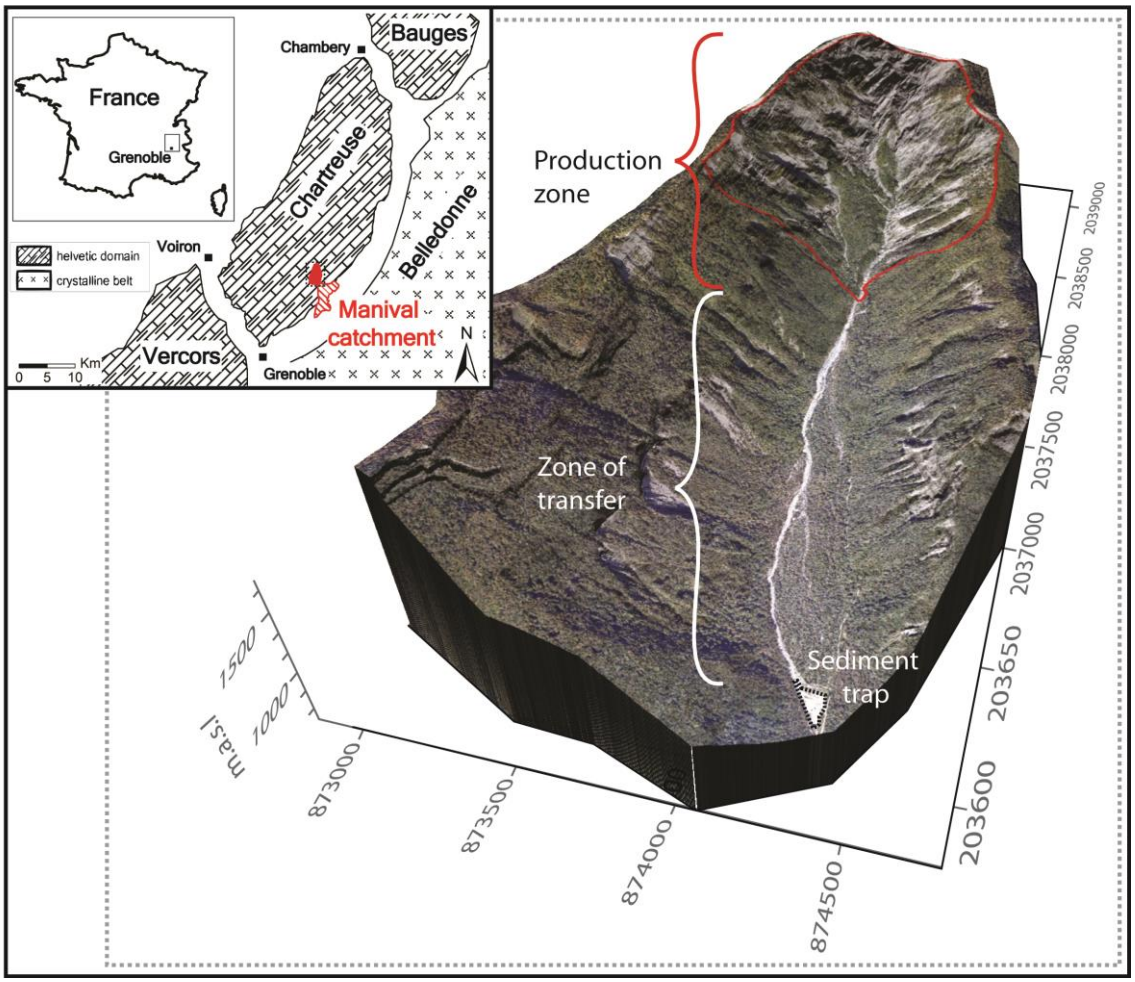

Figure 1. (Inset) Map of the study area; the Manival catchment is in solid red and the impressive debris fan is hatched. (Main) Aerial view of the Manival catchment, draped over a topographic model; sediment supply is concentrated in the headwater (production zone) as erosion activity from the middle and lower catchment is not connected to the torrent (zone of transfer) (image@Aerodata International Surveys; DEM@Irstea UR ETNA).

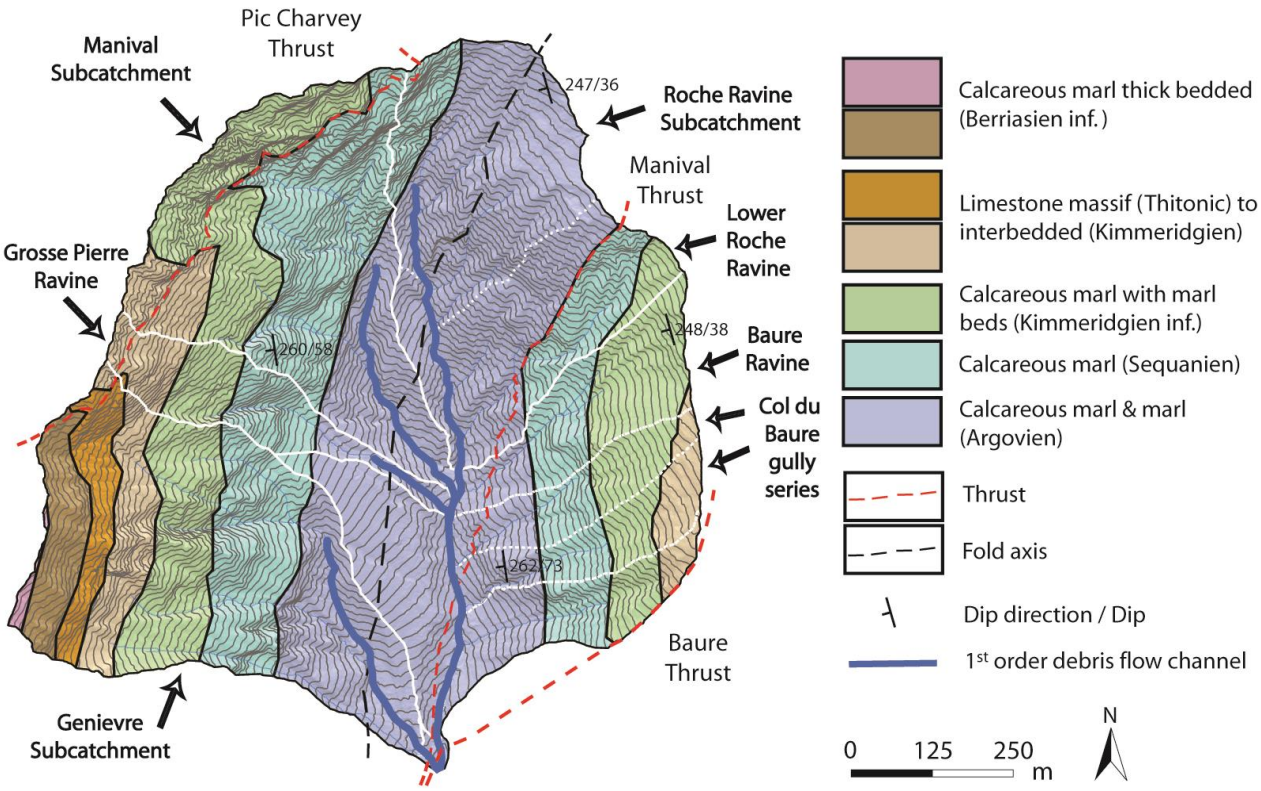

Figure 2. Geological map of the catchment headwater (production zone), after Gidon (1991) and location of first-order debris flow channels (thick blue line) and their respective watersheds (white lines). For the ease of analysis, the Roche Ravine and Col du Baure subcatchments in the east side were further subdivided according to their gully complex (dotted white lines).

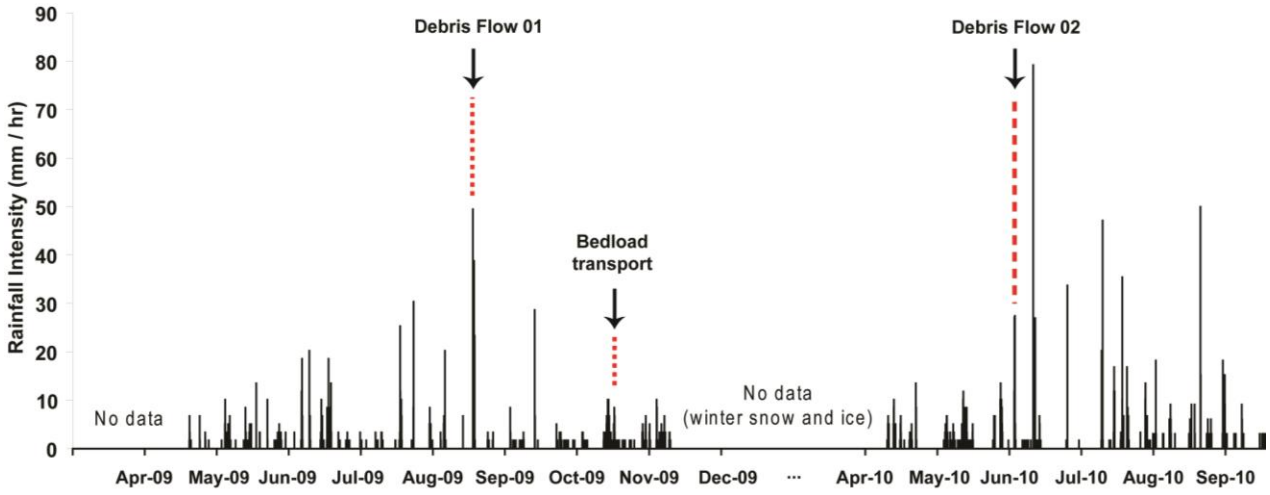

1

2 Figure 3. Maximum rainfall intensity over the monitoring period measured by a rain gauge
3 located at the top of the torrent (see Figure 4) and calculated for a 5 minutes time interval. The
4 mean annual precipitation is about 1,500 mm in the headwater of the Manival (modified from
5 Loye, 2013).

6

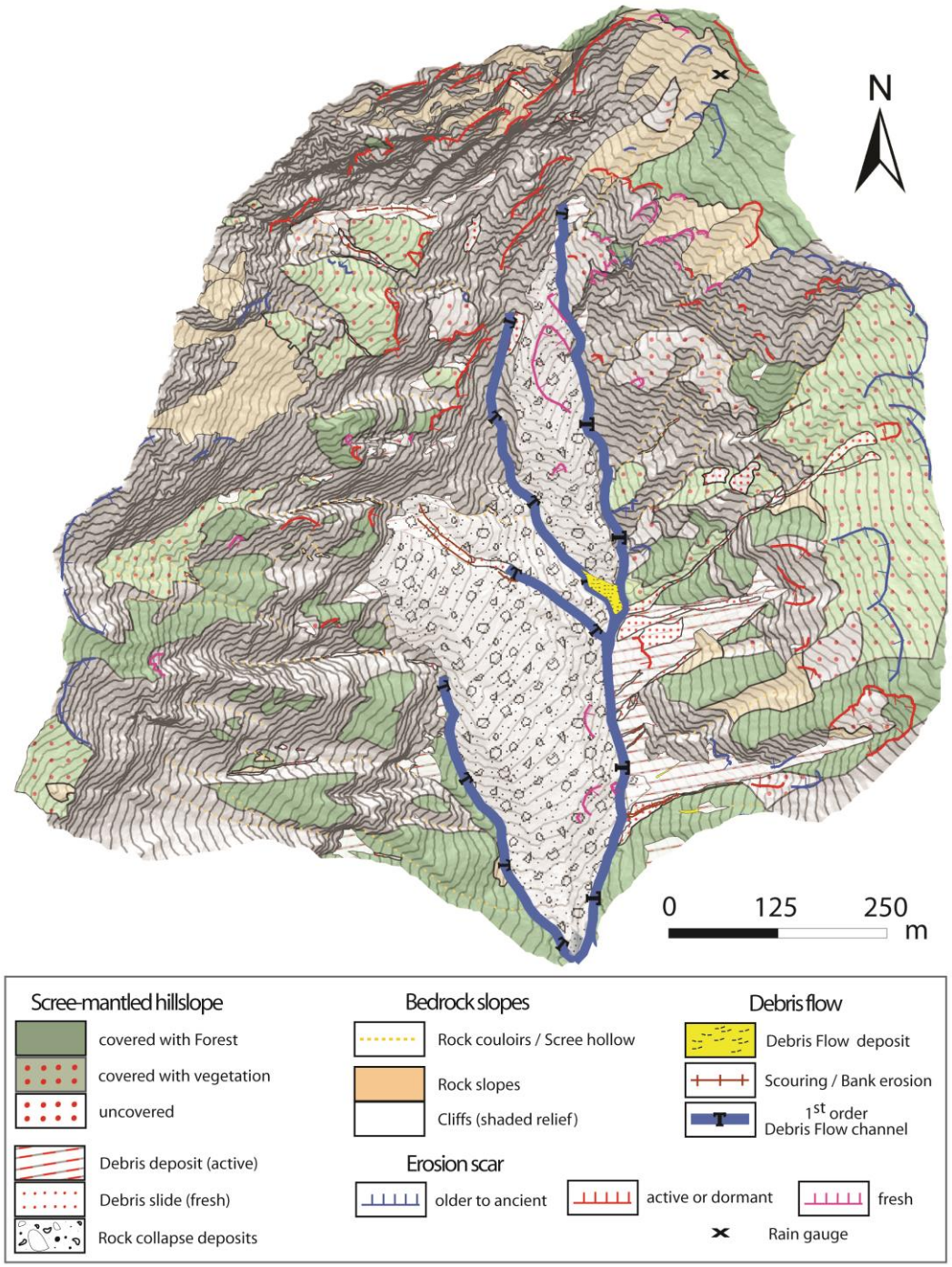

Figure 4. Geomorphic process map (contour interval: 20m) illustrating the spatial pattern of sediment sources and transfer in the first-order channel complex. Note the impressive rock collapse deposits now crossed by four first-order debris channels. Their bed incision is strongly constrained by series of check dams (marked as black "T" on the map), but erosion scars all along the deposit suggest that the reaches are still subject to lateral erosion.

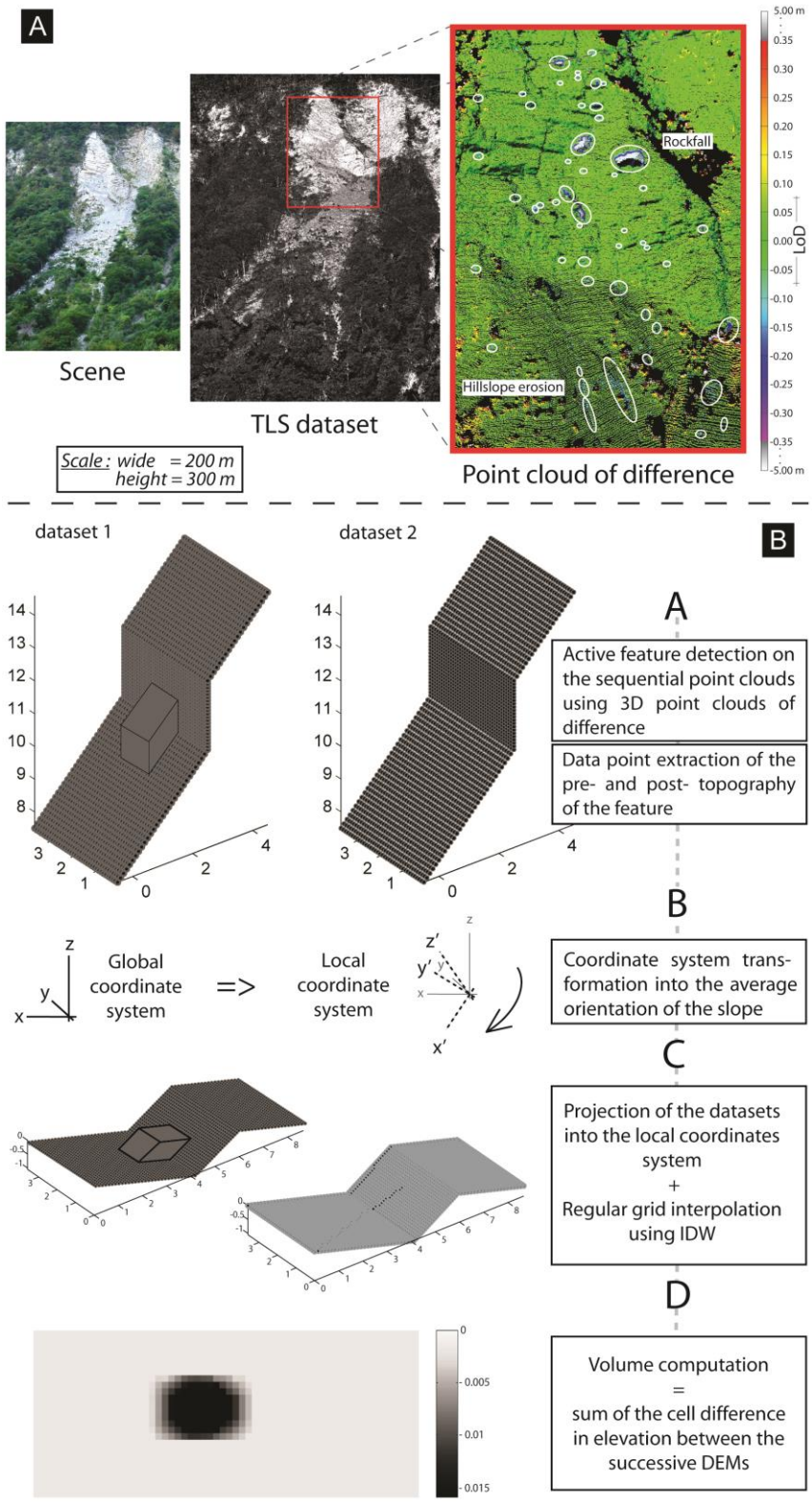

Figure 5. (A) 3-D detection and (B) schematic illustration of the extraction and volume computation method of an individual active feature provided by two successive point cloud datasets.

Histogram Statistics ICP :	Georeferencing Point Cloud April 2009 - July 2010
Subcatch. name	Manival
Mean (μ)	0.000104
Std Dev. (σ)	0.060718
Minimum (min)	-0.212658
Maximum (max)	0.212658
Peak	48593
Number of Points	3526850

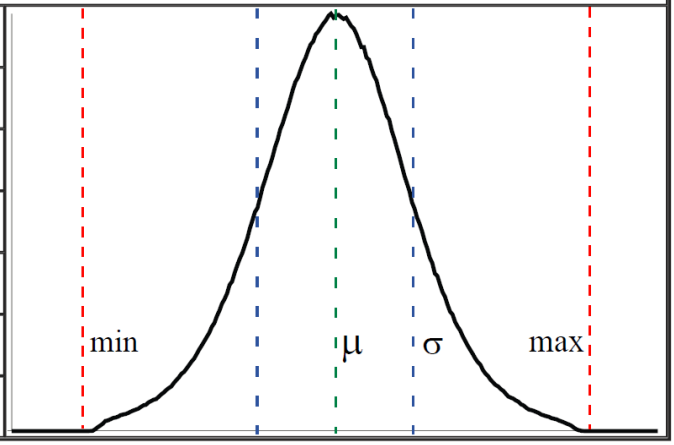

Figure 6. Distribution of the distance between two survey point clouds after the process of georeferencing using ICP procedure. The distance approaches normal distribution with a zero mean, showing that errors generated by multiple scan registration and point cloud survey georeferencing are Gaussian, random and independent. Data are given in meters.

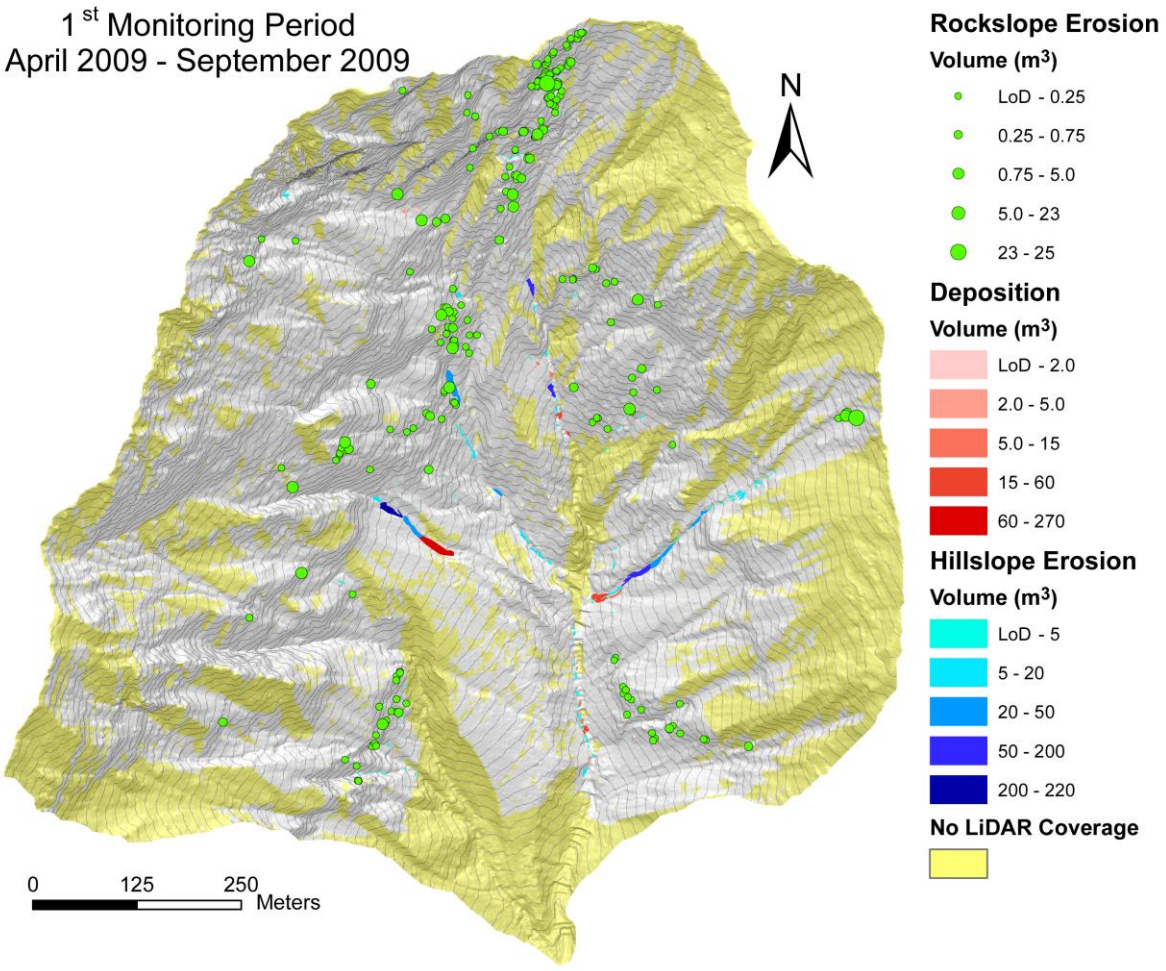

Figure 7. Geomorphic activity revealed by comparing the topographic differences of the two successive TLS surveys operated in April and August 2009. The sediment budgets are detailed for each subcatchment in Fig. 13.

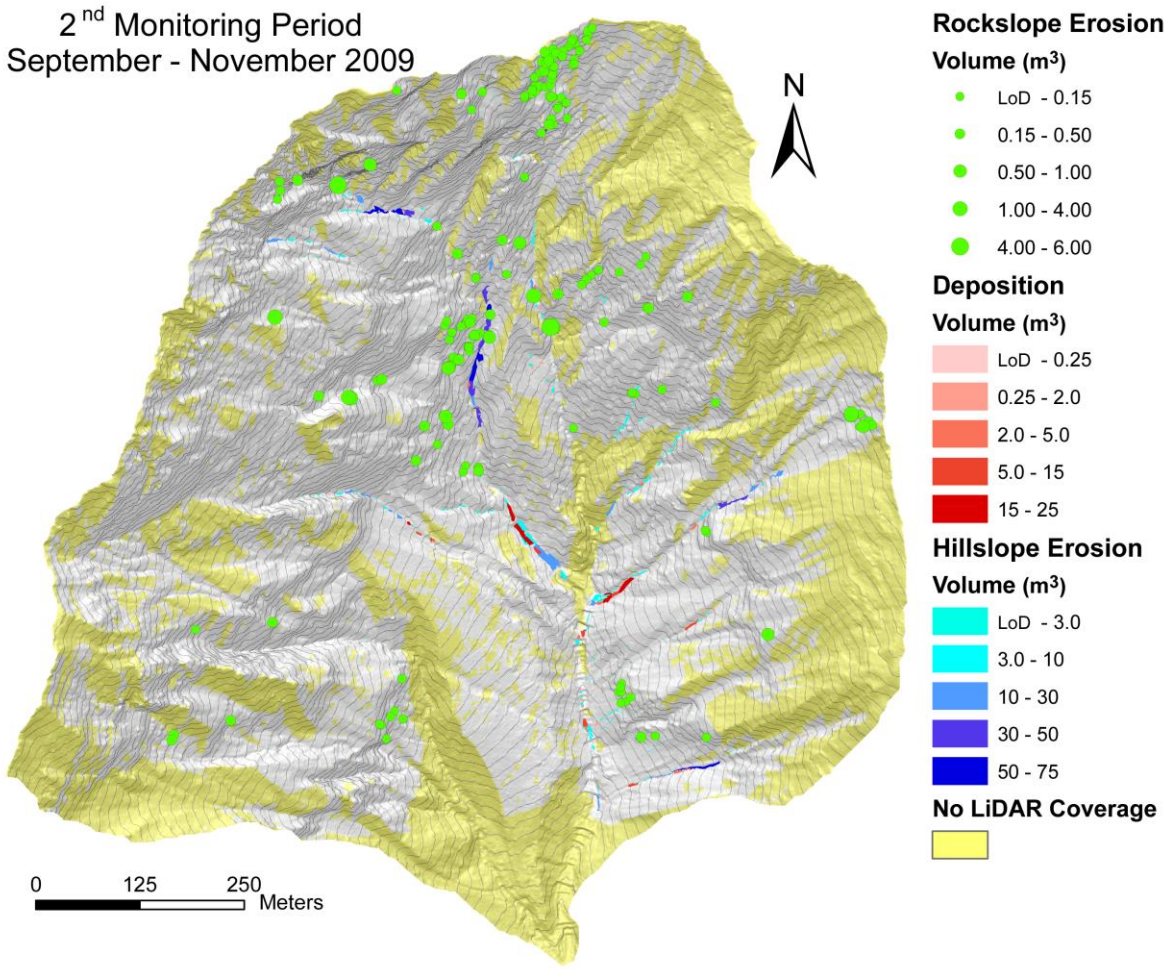

Figure 8. Geomorphic activity revealed by comparing the topographic differences of the two successive TLS surveys operated in August and November 2009. The sediment budgets are detailed for each subcatchment in Fig. 14.

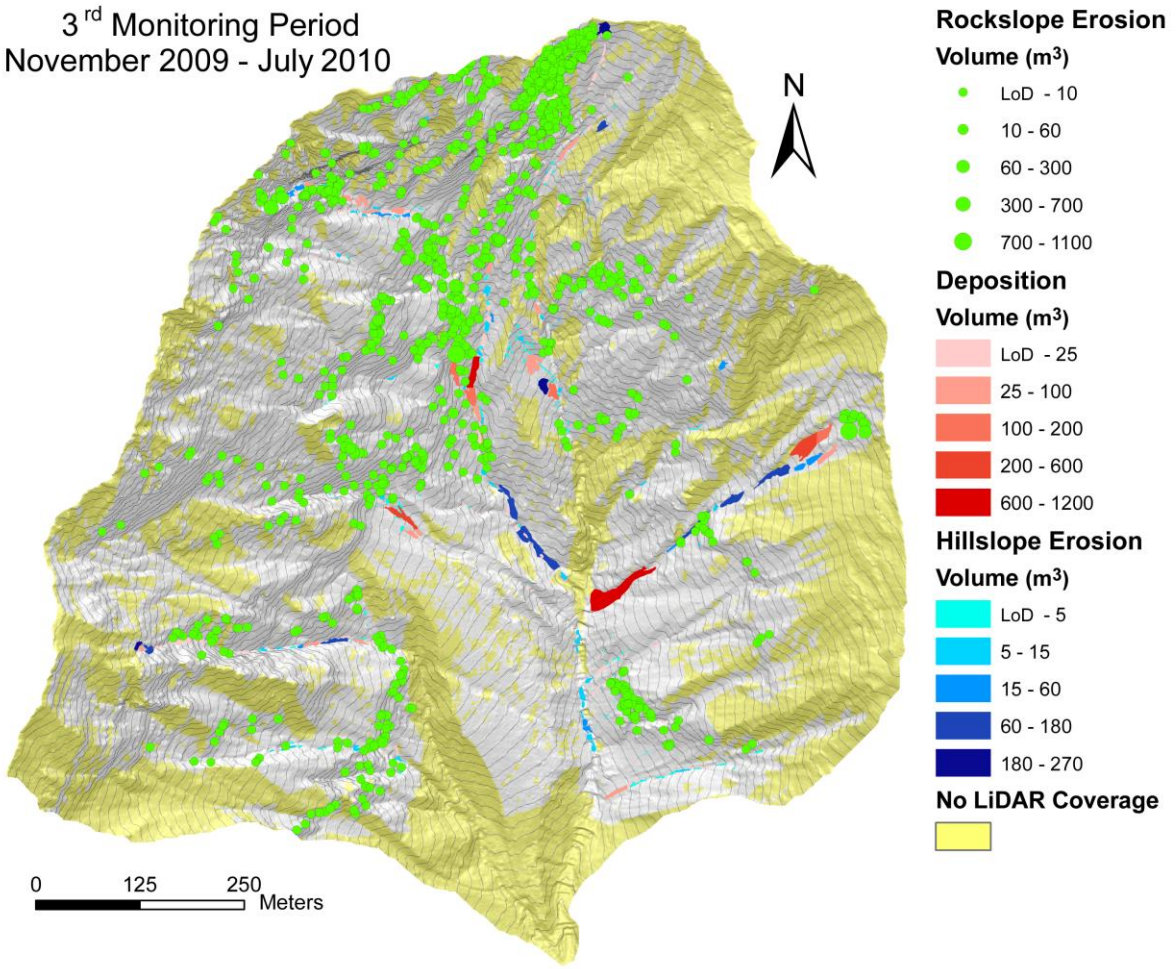

Figure 9. Geomorphic activity revealed by comparing the topographic differences of the two successive TLS surveys operated in November 2009 and July 2010. The sediment budgets are detailed for each subcatchment in Fig. 15.

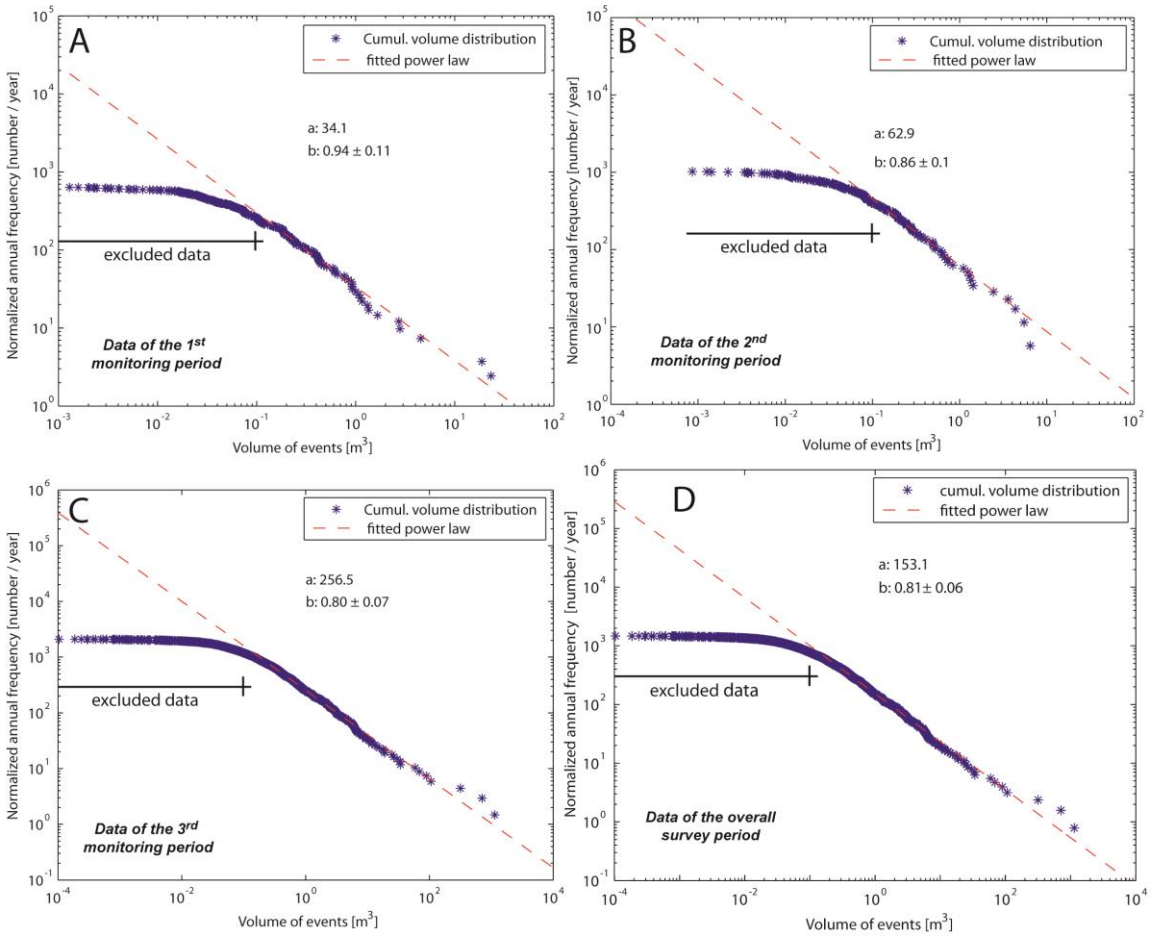

Figure 10. Cumulative volume distribution of the rockfall observed during the first (A), the second (B), the third monitoring period (C) and over the entire study time of 16 months (D). For each dataset, the power law is fitted for volumes larger than 0.1 m^3. Below this threshold volume, the distribution exhibits a roll-over that progressively reaches an almost constant frequency for the smallest detected volumes.

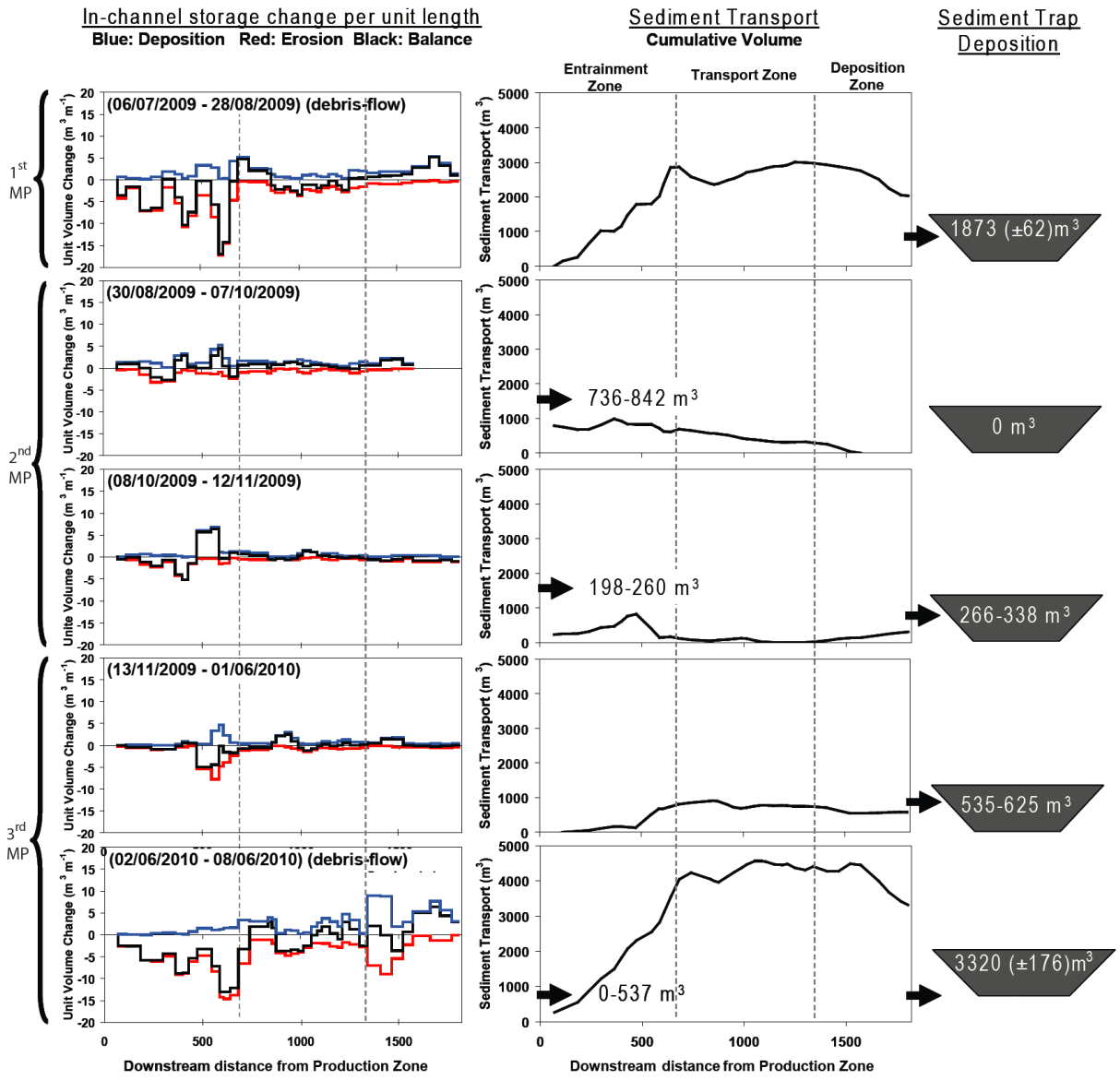

Figure 11. Torrent in-channel storage changes per unit length and sediment budgets of cumulative volumes transported in the torrent from the headwater outlet to the sediment trap downstream for each monitoring period (MP). The torrent recharge (sediment input) was estimated given the in-storage change and the volume deposited in the sediment trap (see Table 4 for details on values) (modified from Theule et al., 2012).

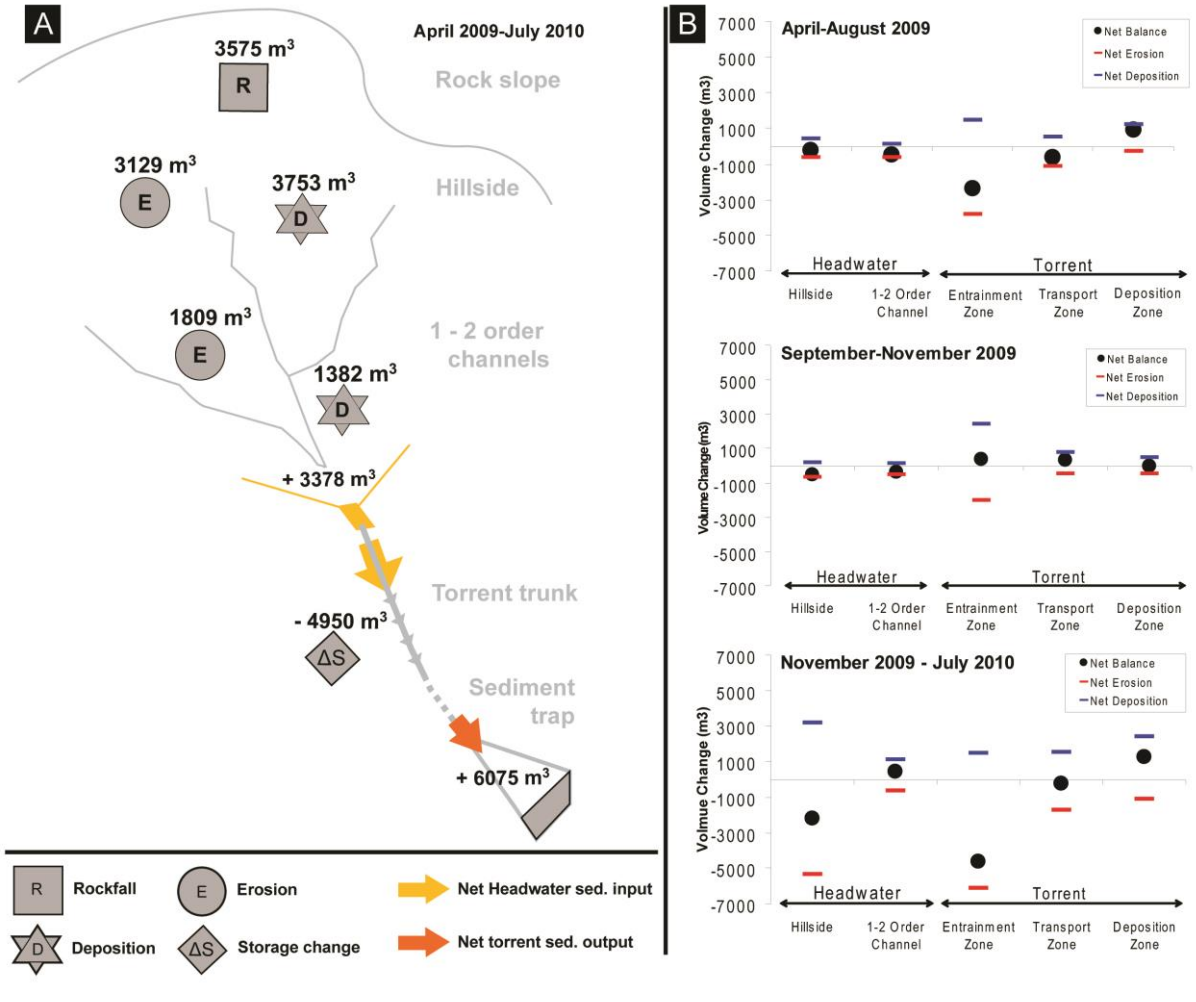

Figure 12. (A) Overall sediment budget and (B) net sediment balance for each monitoring period showing the overall transfer dynamics from debris source zone in the headwater to the apex of the fan through the torrent observed during the period of investigation.

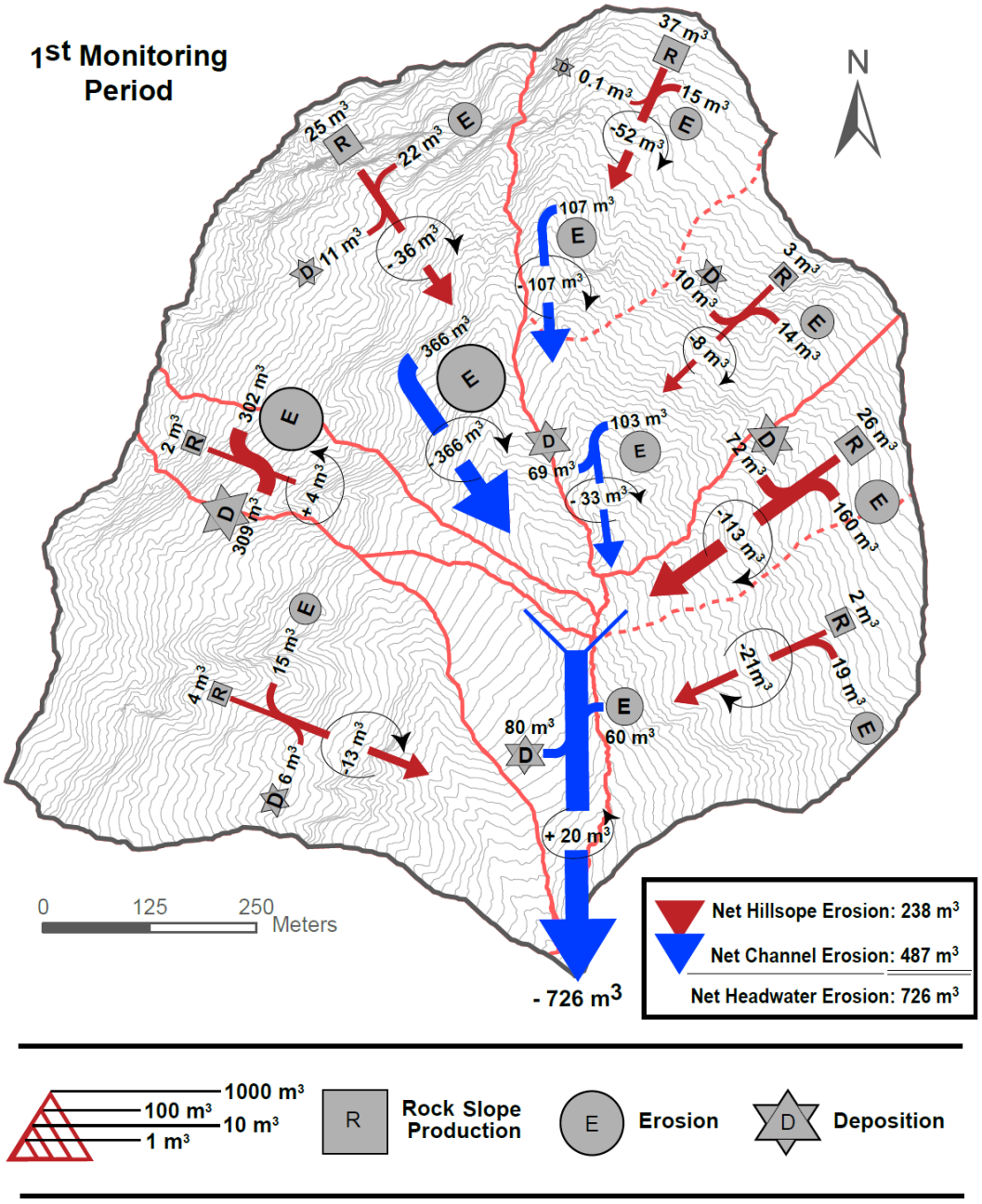

Figure 13. Overall headwater sediment budget observed during the 1st monitoring period revealing the sediment dynamics through the spring-summer season and the net balance of sediment recharge in the downstream torrent for the several months preceding the august 2009 debris flow.

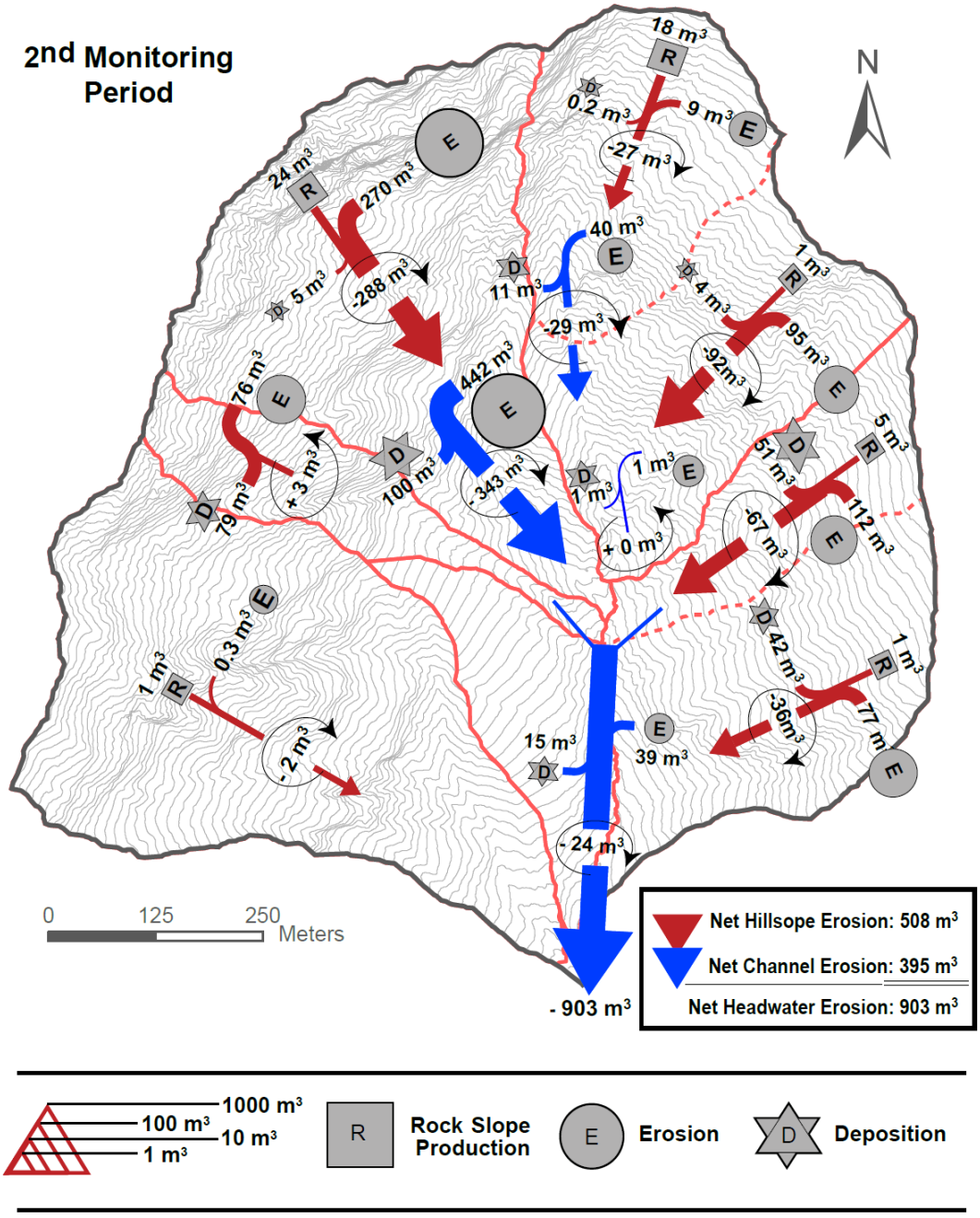

Figure 14. Overall headwater sediment budget observed during the 2nd monitoring period revealing the sediment dynamics and the net balance of sediment recharge in the downstream torrent during the autumn.

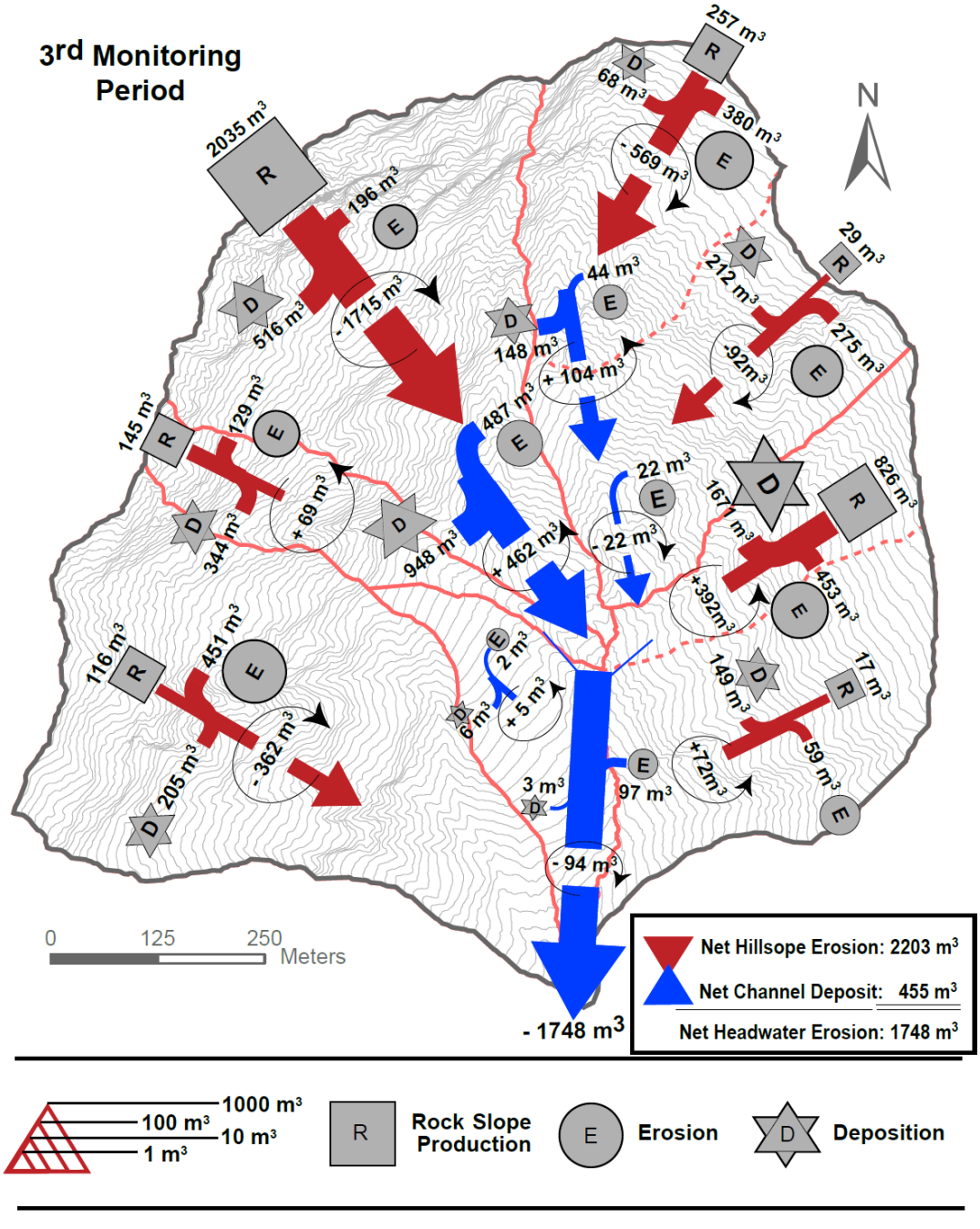

Figure 15. Overall headwater sediment budget observed during the 3rd monitoring period revealing the sediment dynamics through the winter-spring and the net balance of sediment recharge in the downstream torrent for the period preceding the June 2010 debris flow.

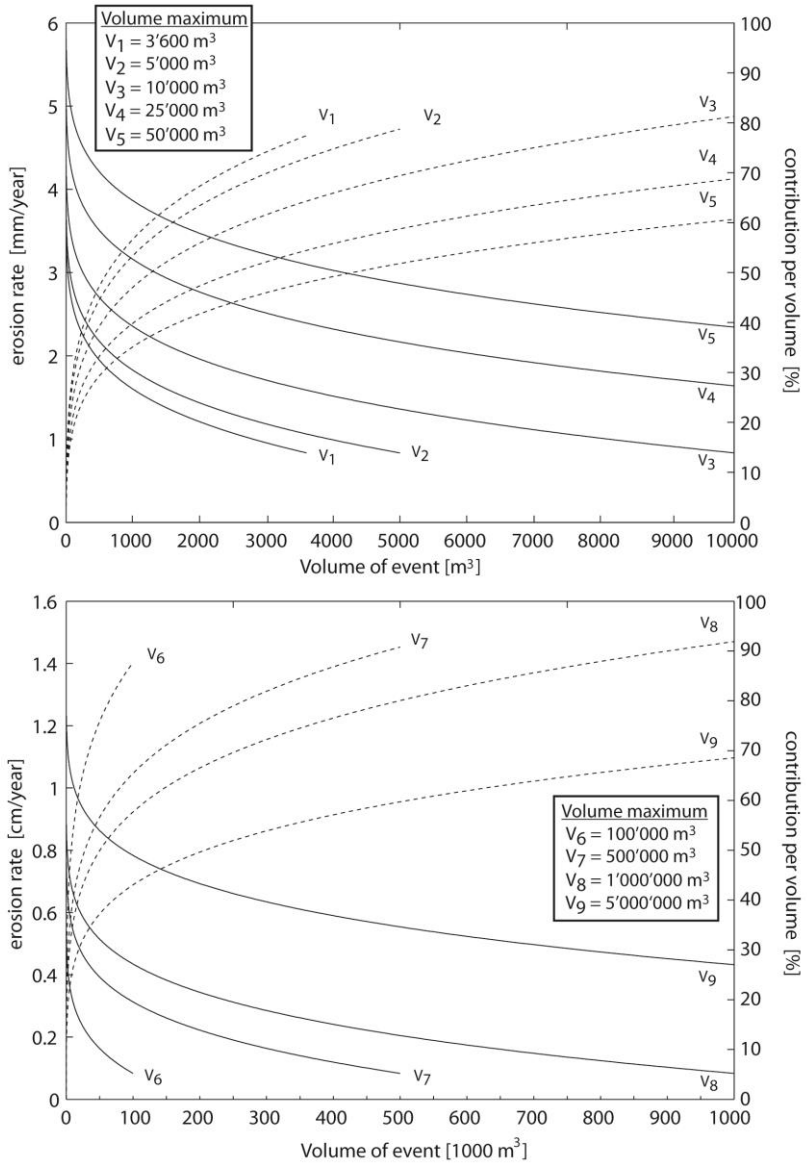

Figure 16. (continuous lines) Erosion rate as function of size of events for a certain volume of production (potential maximum volume $V_{1...9}$), considering that rockfall volume distribution observed at Manival follows power law behaviour (Table 6). (dash lines) Contribution of each class of volumes to the erosion rate showing the significant effect of large slope failures. For a maximum volume eroded of 3,600 m^3/yr (V_1), the 1,000 m^3 rockfall event contributes 60%, while events less than 100 m^3 induce less than 20% of erosion, although of much higher frequency; a 100,000 m^3 rockslide would generate 70% of a total of material eroded of 500,000 m^3 (V_7) over a century.